Table of Contents

1. General Information

Materials. All reagents were used without purification. All solvents were dried with molecular sieves 3Å before use.

Instruments. ^{1}H NMR and ^{13}C NMR spectra were recorded on a Bruker BioSpin DPX400 NMR spectrometer (400 MHz). Chemical shifts were reported in ppm relative to the residual solvent resonances. ESI-TOF MS analyses were performed on a Bruker micrOTOF focus III mass spectrometer. Thernally decomposition temperature (T_d) value of the precursors were determined by thermogravimetry-differential thermal analysis (TG-DTA) using a Mac Science TG-DTA TMA DSC with a heating rate of 10 ºC·min^{-1} in an N_2 stream on platinum pan. The morphologies of the catalysts were investigated by scanning electron microscopy (SEM) using JEOL JSM-7600F with an energy-dispersive X-ray spectroscope (EDX) to obtain elemental mapping images. SEM images, annular dark field scanning transmission electron microscopic (ADF-STEM) images, and bright field scanning transmission electron microscopic (BF-STEM) images in the same field of view of the catalysts were collected by scanning transmission electron microscope (STEM) using HITACHI HD-2000. The atomically dispersed iron species in the catalyst were observed by high-angle annular dark field aberration-corrected scanning transmission electron microscopy (HAADF-STEM) using JEOL JEM-ARM200F equipped with an electron energy loss spectroscopy (EELS). Fe content of each of the Fe/N/C catalysts was characterized by inductively coupled plasma atomic emission spectroscopy (ICP-AES) using a SHIMAZDU ICPS-7510 system. The elemental analysis of carbon, hydrogen and nitrogen was performed on JM10 (J-SCIENCE LAB Co., Ltd.). Raman spectra were obtained using a JASCO NRS3100 instrument with a 532 nm laser. The chemical bonding states of nitrogen species in the catalysts were determined by X-ray photoelectron spectroscopy (XPS) performed on a SHIMADZU KRATOSAXIS-165x. X-ray diffraction (XRD) spectra were measured with Bruker D2 PHASER 2nd Generation with CuKα radiation. Specific surface areas were obtained using a MicrotracBEL BELSORP-mini II analyzer and calculated by Brunauer–Emmett–Teller (BET) method. XAS experiments were performed at the beamline BL12C in Photon Factory (Proposal No. 2021G083).

2. Experimental Procedures

2.1. Synthesis of Precursors

General procedure for synthesis of 1,10-phenanthroline-5,6-dione and compound 2.[1] A mixture of 1,10-phenanthoroline, or 2-(pyridin-2-yl)-1,10-phenanthroline (10 mmol), and KBr (1.79 g, 15 mmol) were slowly added to an ice-cooled mixture of H_2SO_4 (20 mL) and HNO_3 (10 mL). The mixture was refluxed with stirring for 4 h, and then poured onto 100 mL ice-cooled water. The yellow aqueous solution was carefully neutralized with NaOH, then the product was extracted with CH_2Cl_2. The solution was dried over Na_2SO_4, and concentrated to afford the product.

General procedure for synthesis of compounds 1, 3, 6, and 7. To a suspension of 1,10-phenanthroline-5,6-dione derivative (1.25 mmol) and 1,3-diphenylpropane-2-one derivative (1.0 mmol) in dry MeOH (50 mL) was slowly added 1,8-diazabicyclo[5.4.0]undec-7-ene (DBU) (179 μL, 1.2 mmol). The mixture was stirred at room temperature for 24 h. The precipitates were collected and washed with cold MeOH to afford the products.

General procedure for synthesis of compounds L1, L2, L3, and L4.[2] Compound **1**, **3**, **6**, or **7** (0.25 mmol) and 1,2-diphenylacetylene (89.1 mg, 0.5 mmol) were suspended in diphenyl ether (5 mL) and the mixture was deoxygenated by freeze-pump-thaw cycling. The mixture was stirred at 160 ºC under an Ar atmosphere for 24 h. After the mixture was cooled to room temperature, the residues were purified by silica gel column chromatography to afford the product.

Scheme S1. Synthesis of compound **L1**

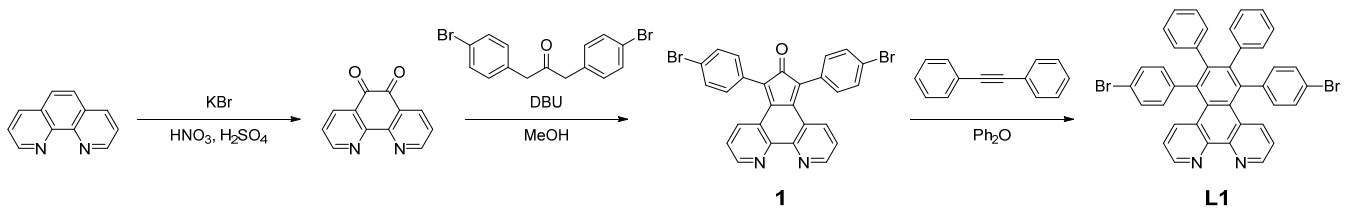

Synthesis of 5,7-bis(4-bromophenyl)-6*H*-cyclopenta[f][1,10]phenanthrolin-6-one (1). 1,10-phenanthroline-5,6-dione (263 mg, 1.25 mmol) and 1,3-bis(4-bromophenyl)propan-2-one (368 mg, 1.0 mmol) were used for the reaction, and compound **1** was obtained as a green solid. Yield 58%. ^{1}H NMR (400 MHz, CD_2Cl_2): δ = 8.86 (dd, 2H, J = 0.8, 4.0 Hz), 7.81 (dd, 2H, J = 0.8, 8.4 Hz), 7.27 (d, 4H, J = 8.4 Hz), 7.10 (dd, 2H, J = 4.4, 8.4 Hz), 7.08 (dd, 2H, J = 4.8, 8.4 Hz); ^{13}C NMR (100 MHz, CD_2Cl_2): δ = 198.91, 152.90, 152.07, 150.75, 146.66, 135.44, 132.55, 131.78, 130.60, 126.23, 124.50, 123.42; ESI-TOF MS (positive mode) m/z calcd. for $C_{27}H_{14}Br_2N_2O$ [M + H]$^+$ 540.9546, found 540.9538.

Synthesis of 5,8-bis(4-bromophenyl)-6,7-diphenyl-1,12-diazatriphenylene (L1). Compound **1** (135 mg, 0.25 mmol) and 1,2-diphenylacetylene (89.1 mg, 0.5 mmol) were used for the reaction, and the product was purified by silica gel column chromatography ($CHCl_3$/MeOH/TEA = 100 : 1 : 1) to afford compound **L1** as a colorless solid. Yield 38%. ^{1}H NMR (400 MHz, CD_2Cl_2): δ = 8.68 (dd, 2H, J = 1.2, 4.4 Hz), 7.83 (dd, 2H, J = 1.2, 4.8 Hz), 7.66 (d, 4H, J = 8.4 Hz), 7.31 (d, 4H, J = 8.4 Hz), 7.08 (dd, 2H, J = 4.4, 4.8 Hz), 6.95 (m, 10H), 6.73 (d, 4H, J = 8.4 Hz); ^{13}C NMR (100 MHz, CD_2Cl_2): δ = 149.38, 147.78, 141.89, 141.34, 139.84, 137.43, 136.81, 133.84, 131.93, 131.62, 129.92, 127.76, 127.30, 126.18, 121.70, 121.40; ESI-TOF MS (positive mode) m/z calcd. for $C_{40}H_{24}Br_2N_2$ [M + H]$^+$ 691.0379, found 691.0384.

Scheme S2. Synthesis of compound **L2**

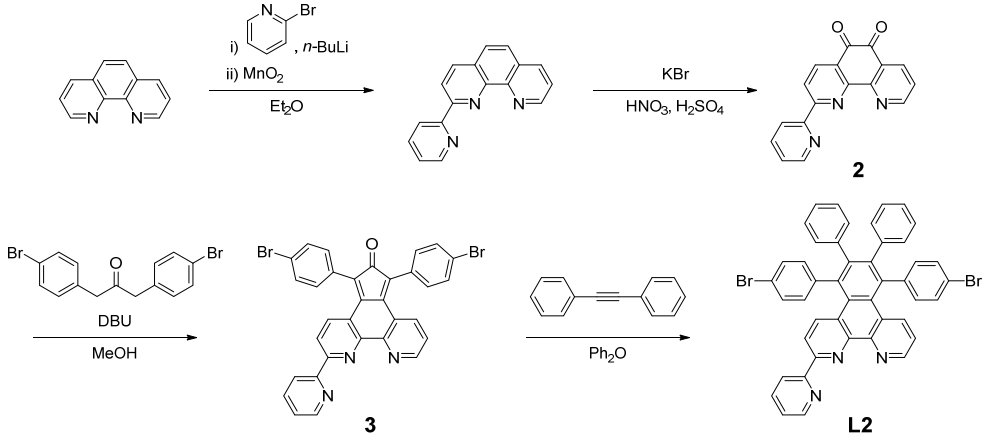

Synthesis of 2-(pyridin-2-yl)-1,10-phenanthroline. According to the procedure described in the literature,[3] 2-(pyridin-2-yl)-1,10-phenanthroline was prepared.

Synthesis of 2-(pyridin-2-yl)-1,10-phenanthroline-5,6-dione (2). 2-(pyridin-2-yl)-1,10-phenanthroline (2.57 g, 10 mmol) was used for the reaction, and compound **2** was obtained as a yellow solid. Yield 71%. ^{1}H NMR (400 MHz, $CDCl_3$): δ = 9.35 (d, 1H, J = 4.0 Hz), 9.07 (d, 1H, J = 8.4 Hz), 9.00 (d, 1H, J = 8.4 Hz), 8.96 (d, 1H, J = 8.4 Hz), 8.78 (d, 1H, J = 4.0 Hz), 8.54 (d, 1H, J = 8.4 Hz), 7.94 (t, 1H, J = 8.0 Hz), 7.84 (dd, 1H, J = 4.0, 4.4 Hz), 7.44 (dd, 1H, J = 4.8, 8.0 Hz); ^{13}C NMR (100 MHz, $CDCl_3$): δ = 159.74, 155.37, 151.68, 149.52, 147.51, 146.50, 144.35, 138.95, 137.41, 132.79, 125.79, 125.69, 125.14, 124.42, 123.34, 122.35, 121.58; ESI-TOF MS (positive mode) m/z calcd. for $C_{17}H_9N_3O_2$ [M + H]$^+$ 288.0768, found 288.0775.

Synthesis of 5,7-bis(4-bromophenyl)-2-(pyridin-2-yl)-6*H*-cyclopenta[f][1,10]phenanthrolin-6-one (3). Compound **2** (359 mg, 1.25 mmol) and 1,3-bis(4-bromophenyl)propan-2-one (368 mg, 1.0 mmol) were used for the reaction, and compound **3** was obtained as a colorless solid. Yield 45%. ^{1}H NMR (400 MHz, DMSO-d_6): δ = 8.81 (d, 1H, J = 4.0 Hz),8.75 (d, 1H, J = 4.0 Hz), 8.66 (d, 1H, J = 8.0 Hz), 8.20 (d, 1H, J = 8.0 Hz), 8.03 (t, 1H, J = 7.6 Hz), 7.96 (d, 1H, J = 7.6 Hz), 7.68 (m, 3H), 7.62 (d, 2H, J = 8.0 Hz), 7.53 (m, 4H), 7.34 (d, 2H, J = 8.0 Hz), 6.44 (s, 1H), 4.77 (s, 1H); ^{13}C NMR (100 MHz, DMSO-d_6): δ = 203.28, 160.63, 157.35, 154.73, 150.16, 149.97, 149.62, 149.37, 137.70, 137.34, 137.09, 136.13, 135.21, 134.52, 132.17, 132.00, 131.69, 131.39, 130.99, 129.87, 125.30, 125.07, 122.46, 121.60, 120.83, 120.39, 74.46, 59.92; ESI-TOF MS (positive mode) m/z calcd. for $C_{32}H_{17}Br_2N_3O$ [M + H_3O]$^+$ 635.9917, found 635.9920.

Synthesis of 5,8-bis(4-bromophenyl)-6,7-diphenyl-2-(2-pyridyl)-1,12-diazatriphenylene (L2). Compound **3** (193 mg, 0.25 mmol) and 1,2-diphenylacetylene (89.1 mg, 0.5 mmol) were used for the reaction, and the prduct was purified by silica gel column chromatography ($CHCl_3$/MeOH/TEA = 100 : 1 : 1) and followed by reprecipitation in a solution of hexane/CH_2Cl_2 to afford compound **L2** as a colorless solid. Yield 25%. ^{1}H NMR (400 MHz, CD_2Cl_2): δ = 8.92 (dd, 2H, J = 1.2, 4.4 Hz), 8.79 (d, 1H, J = 8.0 Hz), 8.68 (d, 1H,

J = 4.0 Hz), 8.20 (d, 1H, *J* = 4.4 Hz), 7.92 (m, 2H), 7.84 (dd, 1H, *J* = 1.2, 8.0 Hz), 7.37 (dd, 1H, *J* = 1.2, 6.0 Hz), 7.29 (dd, 4H, *J* = 3.6, 8.4 Hz), 7.14 (dd, 1H, *J* = 4.4, 4.8 Hz), 6.98 (m, 10H), 6.74 (m, 4H); ^{13}C NMR (100 MHz, CD_2Cl_2): *δ* = 155.92, 154.70, 149.23, 148.91, 147.36, 146.80, 141.59, 141.57, 140.94, 140.87, 139.45, 137.46, 137.16, 137.04, 136.95, 136.60, 133.45, 131.58, 131.54, 131.23, 129.64, 127.73, 127.56, 126.91, 125.79, 124.05, 121.69, 121.32, 121.11, 121.01, 118.68; ESI-TOF MS (positive mode) *m*/*z* calcd. for $C_{45}H_{27}Br_2N_3$ $[M + H]^+$ 786.0512, found 786.0513.

Scheme S3. Synthesis of compound **L3**

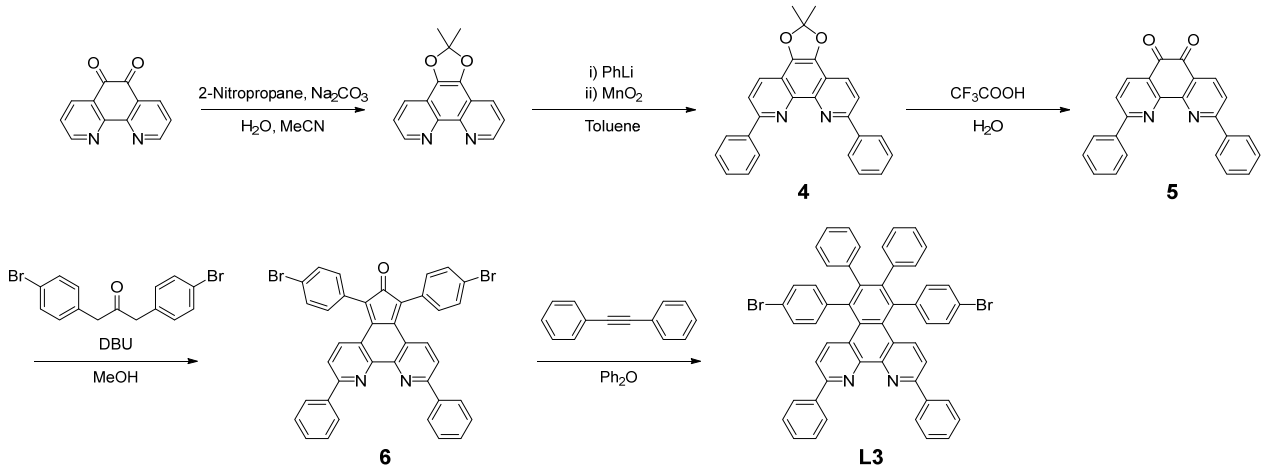

Synthesis of 2,2-dimethyl-6,9-diphenyl-[1,3]dioxolo[4,5-f][1,10]phenanthroline (4). Compound **4** was synthesized according to the literature with some modifications.[4] A solution of 2,2-dimethyl-[1,3]dioxolo[4,5-f][1,10]phenanthroline (4.0 g, 15.9 mmol) in dry and degassed toluene (150 mL) was cooled to 0 ºC under an Ar atmosphere and stirred vigorously. The mixture was slowly added a solution of 1.2 equivalent of phenyllithium (1.9 mol·L^{-1}) in *n*-butyl ether (10 mL, 19 mmol) and the mixture was stirred for 2 h. The reaction was quenched by adding H_2O (30 mL) and the product was extracted with CH_2Cl_2. To the solution was added MnO_2 (15 g) and the mixture was stirred for 2 h. After the precipitates were filtered through celite, the solution was concentrated *in vacuo* to afford a mono-substituted compound. The same procedure was performed again to obtain compound **4** as a red oil. Yield 92%. ^{1}H NMR (400 MHz, $CDCl_3$): *δ* = 8.45 (d, 4H, *J* = 7.6 Hz), 8.32 (d, 2H, *J* = 8.4 Hz), 8.15 (d, 2H, *J* = 8.4 Hz), 7.59 (t, 4H, *J* = 7.6 Hz), 7.48 (t, 2H, *J* = 7.6 Hz), 1.91 (s, 6H); ^{13}C NMR (100 MHz, $CDCl_3$): *δ* = 154.57, 142.49, 139.74, 136.66, 129.31, 128.96, 127.59, 120.82, 119.88, 117.47, 26.29; ESI-TOF MS (positive mode) *m*/*z* calcd. for $C_{27}H_{22}N_2O_2$ $[M + H]^+$ 407.1754, found 407.1749.

Synthesis of 2,9-diphenyl-1,10-phenanthroline-5,6-dione (5). Compound **5** was synthesized according to the literature with some modifications.[5] Compound **4** (2.0 g, 5.0 mmol) was dissolved in a mixture of water (25 mL) and trifluoroacetic acid (50 mL), and the mixture was stirred at 50 ºC for 5 h under aerobic conditions. After the mixture was cooled to room temperature, the solvents were evaporated *in vacuo*. The residue was extracted with CH_2Cl_2 and washed with an aqueous solution of $NaHCO_3$ (1.0 mol·L^{-1}) and water. The organic layer was dried over $NaSO_4$, and the solvent was evaporated *in vacuo* to afford compound **5**. Yield 85%. ^{1}H NMR (400 MHz, $CDCl_3$): *δ* = 8.54 (d, 2H, *J* = 8.4 Hz), 8.36 (dd, 4H, *J* = 1.2, 8.4 Hz), 8.02 (d, 2H, *J* = 8.4 Hz), 7.58 (m, 6H); ^{13}C NMR (100 MHz, $CDCl_3$): *δ* = 179.97, 163.10, 153.13, 138.19, 137.79, 131.25, 129.28, 128.06, 126.85, 121.58; ESI-TOF MS (positive mode) *m*/*z* calcd. for $C_{24}H_{14}N_2O_2$ $[M + H]^+$ 363.1128, found 363.1128.

Synthesis of 5,7-bis(4-bromophenyl)-2,10-diphenyl-6*H*-cyclopenta[f][1,10]phenanthrolin-6-one (6). Compound **5** (453 mg, 1.25 mmol) and 1,3-bis(4-bromophenyl)propan-2-one (368 mg, 1.0 mmol) were used for the reaction, and the crude products containing compound **6** were obtained as a brown solid. The crude products were used for synthesis of compound **L3** without further purification. ESI-TOF MS (positive mode) *m*/*z* calcd. for $C_{39}H_{22}Br_2N_2O$ $[M + H_3O]^+$ 711.0277, found 711.0280.

Synthesis of 5,8-bis(4-bromophenyl)-2,6,7,11-tetraphenyl-1,12-diazatriphenylene (L3). Compound **6** (174 mg, 0.25 mmol) and 1,2-diphenylacetylene (89.1 mg, 0.5 mmol) were used for the reaction, and the prduct was purified by silica gel column chromatography ($CHCl_3$/MeOH/TEA = 100 : 1 : 1). The product was precipitated from hexane/CH_2Cl_2 to afford compound **L3** as a colorless solid. Yield 28%. ^{1}H NMR (400 MHz, $CDCl_3$): *δ* = 8.41 (d, 4H, *J* = 8.0 Hz), 7.83 (d, 2H, *J* = 8.8 Hz), 7.63 (d, 2H, *J* = 8.8 Hz), 7.56 (t, 4H, *J* = 7.2 Hz), 7.48 (d, 2H, *J* = 7.2 Hz), 7.28 (d, 4H, *J* = 8.0 Hz), 6.95 (m, 10H), 6.70 (d, 2H, *J* = 7.2 Hz); ^{13}C NMR (100 MHz, $CDCl_3$): *δ* = 155.72, 147.29, 141.36, 140.97, 139.43, 138.92, 137.62, 137.06, 133.51, 131.82, 131.34, 129.74, 129.60, 128.92, 127.45, 127.20, 126.53, 126.02, 121.33, 118.13; ESI-TOF MS (positive mode) *m*/*z* calcd. for $C_{52}H_{32}Br_2N_2$ $[M + H]^+$ 843.1005, found 843.1013.

Scheme S5. Synthesis of compound **L4**

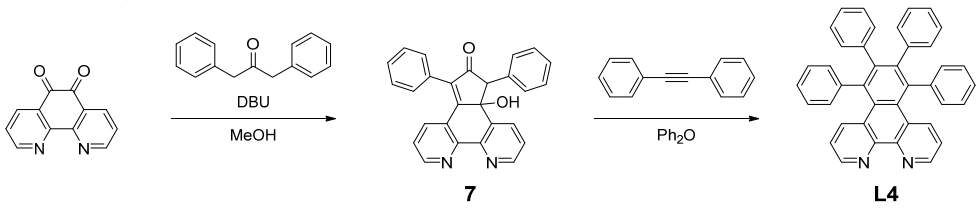

Synthesis of 4b-hydroxy-5,7-diphenyl-4b,5-dihydro-6*H*-cyclopenta[f][1,10]phenanthrolin-6-one (7). 1,10-phenanthroline-5,6-dione (263 mg, 1.25 mmol) and 1,3-diphenylpropane-2-one (210 mg, 1.0 mmol) were used for the reaction, and compound **7** was obtained as a colorless solid. Yield 45%. ^{1}H NMR (400 MHz, $CDCl_3$): δ = 8.83 (d, 1H, J = 4.4 Hz), 8.79 (d, 1H, J = 4.4 Hz), 8.04 (d, 1H, J = 7.6 Hz), 8.04 (d, 1H, J = 7.6 Hz), 7.49 (m, 4H), 7.42 (m, 3H), 7.16 (dd, 1H, J = 4.4, 7.6 Hz), 4.51 (s, 1H), 2.45 (s, 1H); ^{13}C NMR (100 MHz, $CDCl_3$): δ = 202.84, 158.86, 152.69, 151.03, 150.39, 150.30, 140.39, 136.66, 136.57, 135.00, 134.07, 132.03, 129.99, 129.25, 129.19, 129.08, 129.05, 128.40, 125.35, 124.77, 123.75, 74.93, 61.08; ESI-TOF MS (positive mode) m/z calcd. for $C_{27}H_{18}N_2O_2$ $[M + H]^+$ 403.1441, found 403.1440.

Synthesis of 5,6,7,8-tetraphenyl-1,12-diazatriphenylene (L4). Compound **7** (101 mg, 0.25 mmol) and 1,2-diphenylacetylene (89.1 mg, 0.5 mmol) were used for the reaction, and the prduct was purified by silica gel column chromatography ($CHCl_3$/MeOH/TEA = 100 : 1 : 1). The product was precipitated from hexane/CH_2Cl_2 to afford compound **L4** as a colorless solid. Yield 47%. ^{1}H NMR (400 MHz, $CDCl_3$): δ = 8.90 (d, 2H, J = 4.4 Hz), 7.80 (d, 2H, J = 8.8 Hz), 7.13 (m, 6H), 7.04 (m, 4H), 7.01 (d, 2H, J = 4.4 Hz), 6.89 (m, 6H), 6.70 (m, 4H); ^{13}C NMR (100 MHz, $CDCl_3$): δ = 149.22, 147.46, 142.01, 141.58, 139.88, 138.30, 136.90, 131.89, 131.43, 129.63, 128.56, 127.93, 126.94, 126.89, 125.67, 121.39; ESI-TOF MS (positive mode) m/z calcd. for $C_{40}H_{26}N_2$ $[M + H]^+$ 535.2169, found 535.2174.

The thermal durability of the ligands (**L1**−**L6**) were determined by thermal gravimetric analysis (Figure S1).

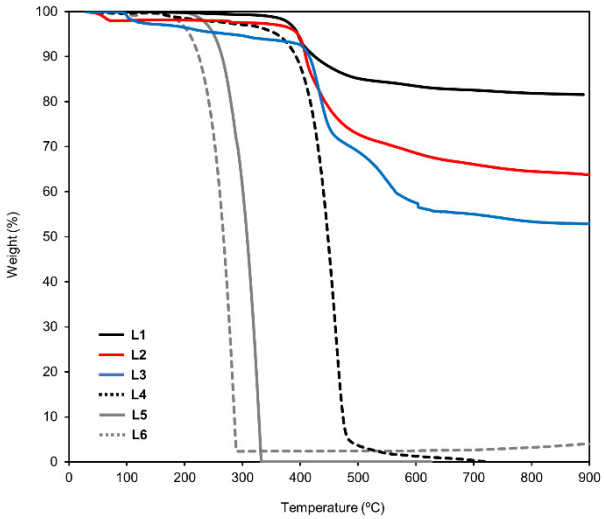

Figure S1. Thermal gravimetric analysis curves of **L1** (black solid line), **L2** (red solid line), **L3** (blue solid line), **L4** (black dashed line), **L5** (gray solid line), **L6** (gray dashed line).

Synthesis of Fe complex ([Fe(L1)$_3$](ClO$_4$)$_2$). A solution of compound **L1** (208 mg, 0.3 mmol) in $CHCl_3$ (50 mL) and a solution of $Fe(ClO_4)_2{\cdot}6H_2O$ (36.3 mg, 0.1 mmol) in MeOH (10 mL) were combined and the mixture was stirred for 2 h at room temperature under an N_2 atmosphere. Then, the obtained precipitates were filtered and washed with a small amount of MeOH and Et_2O to afford the iron complex [Fe(**L1**)$_3$](ClO$_4$)$_2$ as a red solid. The complexation was confirmed by UV-vis titration experiment (Figure S2) and single crystals for X-ray crystal structure analysis were grown from MeCN/Et_2O by gas-liquid diffusion method (Figure 2b).

Synthesis of Fe complex ([Fe(L2)$_2$](ClO$_4$)$_2$). A solution of compound **L2** (154 mg, 0.2 mmol) in $CHCl_3$ (50 mL) and a solution of $Fe(ClO_4)_2{\cdot}6H_2O$ (36.3 mg, 0.1 mmol) in MeOH (10 mL) were combined and the mixture was stirred for 2 h at room temperature under an N_2 atmosphere. Then, the obtained precipitates were filtered and washed with a small amount of MeOH and Et_2O to afford the iron complex [Fe(**L2**)$_2$](ClO$_4$)$_2$ as a purple solid. The complexation was confirmed by UV-vis titration experiment (Figure S3) and single crystals for X-ray crystal structure analysis were grown from MeCN/Et_2O by gas-liquid diffusion method (Figure 2c).

Synthesis of Fe complex ([Fe(L4)$_3$](ClO$_4$)$_2$). A solution of compound **L4** (160 mg, 0.3 mmol) in $CHCl_3$ (50 mL) and a solution of $Fe(ClO_4)_2{\cdot}6H_2O$ (36.3 mg, 0.1 mmol) in MeOH (10 mL) were combined and the mixture was stirred for 2 h at room temperature under an N_2 atmosphere. Then, the obtained precipitates were filtered and washed with small amount of MeOH and Et_2O to afford the iron

complex [Fe(**L4**)$_3$](ClO$_4$)$_2$ as a red solid. Single crystals for X-ray crystal structure analysis were grown from MeCN/Et$_2$O by gas-liquid diffusion method (Figure S5).

Preparation of the mixture of Fe ion and compound L3. A solution of compound **L3** (253 mg, 0.3 mmol) in $CHCl_3$ (50 mL) and a solution of Fe(ClO$_4$)$_2$·6H$_2$O (36.3 mg, 0.1 mmol) in MeOH (10 mL) were combined and the mixture was stirred for 2 h at room temperature. Then, the solvents were evaporated in vacuo to afford the mixture of Fe ion and compound **L3**.

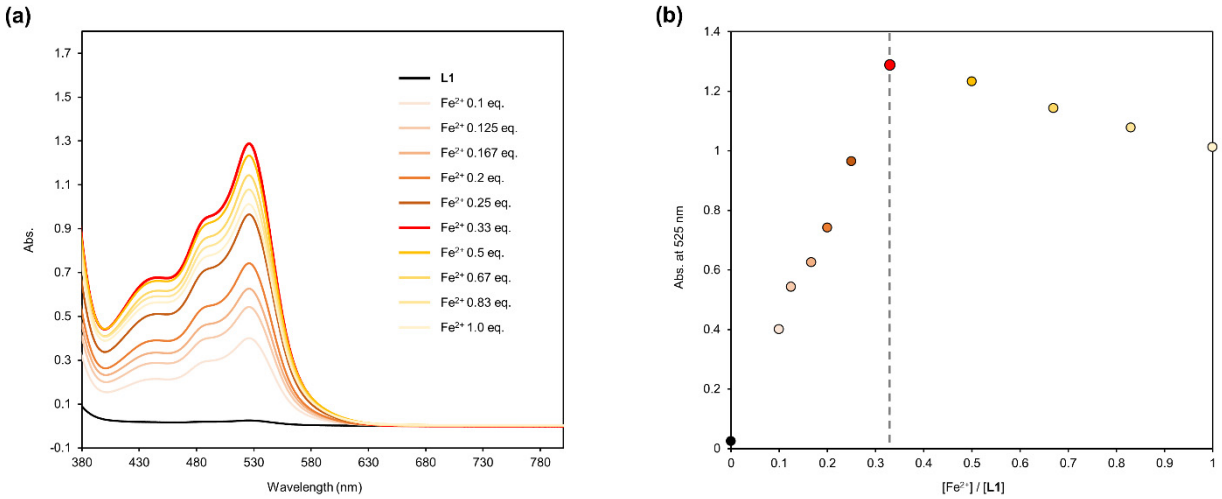

Figure S2. (a) UV-vis titration spectra of **L1** vs Fe^{2+} in $CHCl_3$. (b) Plots of absorbance at 525 nm against the ratio of [Fe^{2+}] / [**L1**].

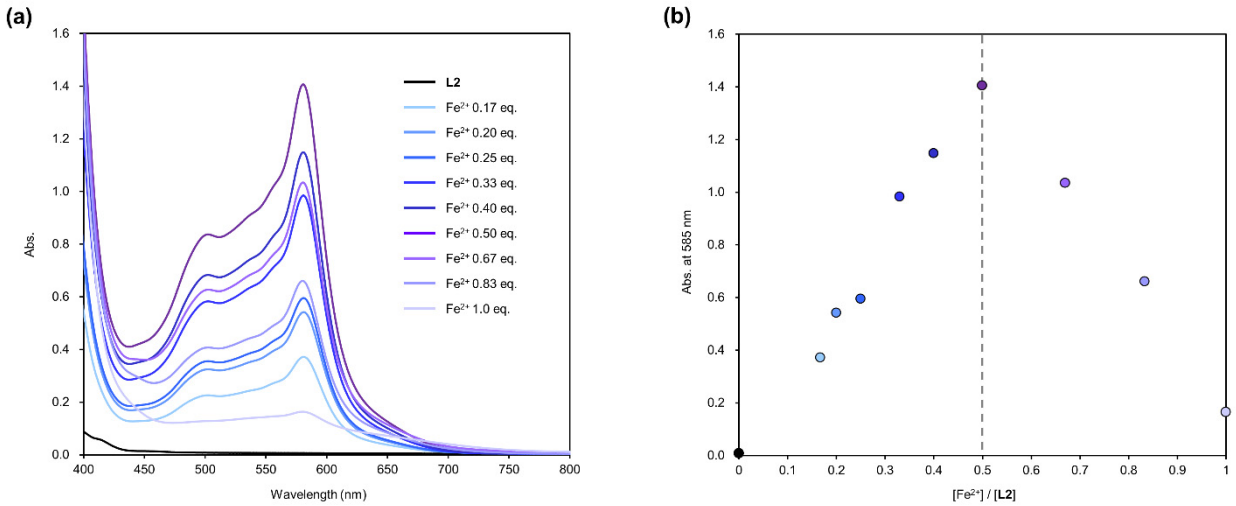

Figure S3. (a) UV-vis titration spectra of **L2** vs Fe^{2+} in $CHCl_3$. (b) Plots of absorbance at 585 nm against the ratio of [Fe^{2+}] / [**L2**].

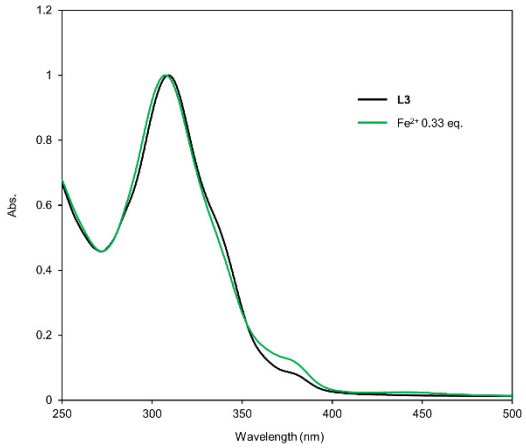

Figure S4. UV-vis spectra of **L3** (black) and **L3** with Fe^{2+} (0.33 eq.) (green) in $CHCl_3$.

2.2. X-ray Crystal Structures of the Precursors

Diffraction data of the Fe complexes were collected on a two-dimensional X-ray detector (PILATUS 200K/R) equipped in Rigaku XtaLAB P200 diffractometer using multi-layer mirror monochromated Cu-Kα radiation (λ = 1.54187 Å) at 223 or 93 K. Diffraction Data collection, cell refinement, and data reduction were carried out with CrysAlis PRO.[6] SHELXT[7] was used for the structure solution of the crystals. These calculations were performed with the observed reflections [$I > 2\sigma(I)$] with the program CrystalStructure crystallographic software.[8] Structural refinement was performed by SHELXL.[9] All non-hydrogen atoms were refined with anisotropic displacement parameters, and hydrogen atoms were placed in idealized positions and refined as rigid atoms with the relative isotropic displacement parameters. SQUEEZE function equipped in the PLATON program was used to treat severely disordered solvent molecules in voids.[10]

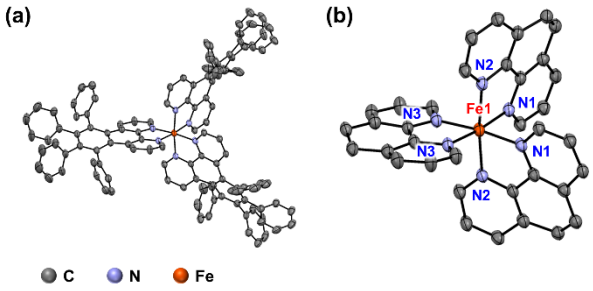

Figure S5. X-ray crystal structures of (a) $[Fe(\mathbf{L4})_3]^{2+}$ with 50% thermal ellipsoid probability (Hydrogen atoms, solvents and the non-bonding counter anion (ClO_4^-) are omitted for clarity.). Enlarged views around the iron center of (b) $[Fe(\mathbf{L4})_3]^{2+}$: selected bond length [Å]: Fe1−N1 1.980; Fe1−N2 1.960; Fe1−N3 1.964.

Table S1. Summary of Crystallographic Data for the Iron Complexes.

	$[Fe(\mathbf{L1})_3](ClO_4)_2$	$[Fe(\mathbf{L2})_2](ClO_4)_2$	$[Fe(\mathbf{L4})_3](ClO_4)_2$
Experimental formula	$C_{120}H_{72}Br_6Cl_2FeN_6O_8$	$C_{90}H_{54}Br_4Cl_2FeN_6O_8$	$C_{128}H_{98}Cl_2FeN_6O_{10}$
Formula weight	2332.10	1793.82	2006.97
Crystal system	monoclinic	monoclinic	monoclinic
a (Å)	24.8276(4)	19.6101(11)	27.4633(5)
b (Å)	21.75740(17)	18.9123(11)	20.1049(5)
c (Å)	26.8552(4)	24.0069(10)	18.9421(5)
α (deg)	90	90	90
β (deg)	114.8860(18)	102.627(5)	95.9287(19)
γ (deg)	90	90	90
V (Å^3)	13159.8(4)	8688.1(8)	10402.9(4)
Space group	*P* $2_1/n$	*I* 2/*a*	*C* 2/*c*
Z	4	4	4
ρ_{calc} (g·cm^{-3})	1.177	1.371	1.281
m (CuK*a*) (cm^{-1})	3.819	4.573	2.159
Temp. (K)	223	93	93
Data	80108	30481	30194
Unique data	26140	8608	10272
R_1	5.60	11.13	8.49
wR_2	17.33	34.23	26.52
GOF	1.074	0.989	1.092

2.3. Preparation of the Fe/N/C catalysts

Carbon black Vulcan® XC-72R (VC, Cabot, USA) was used as a carbon support. The catalysts were prepared from the iron complexes, $Fe(\mathbf{L1})_3$, $Fe(\mathbf{L2})_2$, $Fe(\mathbf{L4})_3$, $Fe(\mathbf{L5})_3$, $Fe(\mathbf{L6})_3$, or the mixture of **L3** and iron ion with VC by pyrolysis in N_2 gas flow; Their names are abbreviated as Fe/**L1**@VC, Fe/**L2**@VC, Fe/**L4**@VC, Fe/**L5**@VC, and Fe/**L6**@VC, and Fe/**L3**@VC, respectively. The Fe/N/C catalysts were prepared as follows: One of the Fe complexes or a mixture of **L3** and Fe^{2+} (0.05 mmol) was dissolved in CH_2Cl_2 (50 mL) and mixed with a powder of VC (100 mg). The suspension was vigorously vortexed and sonicated for 30 min, and then the solvent was removed. The obtained mixture was placed on an alumina boat (length: 80 mm, width: 16 mm, height: 10 mm) which was then placed in a quartz tube (diameter 50 mm, length 800 mm). The quartz tube was installed in a hinge split tube furnace (Koyo Thermo Systems Co. Ltd., KTF045N1). The mixture was heated from ambient temperature to 700 ºC (heating rate is 2 ºC·min^{-1}) for 2h under N_2 flow (0.2 L·min^{-1}) and incubated for 2h. The temperature of the sample inside the furnace was recorded with a thermocouple equipped with a data logger (CHINO Corporation, MC3000). After cooling to ambient temperature, the pyrolyzed materials were ground to be uniform, and then, the Fe/N/C catalyst was obtained.

2.4. Characterizations

Raman spectrometric analysis

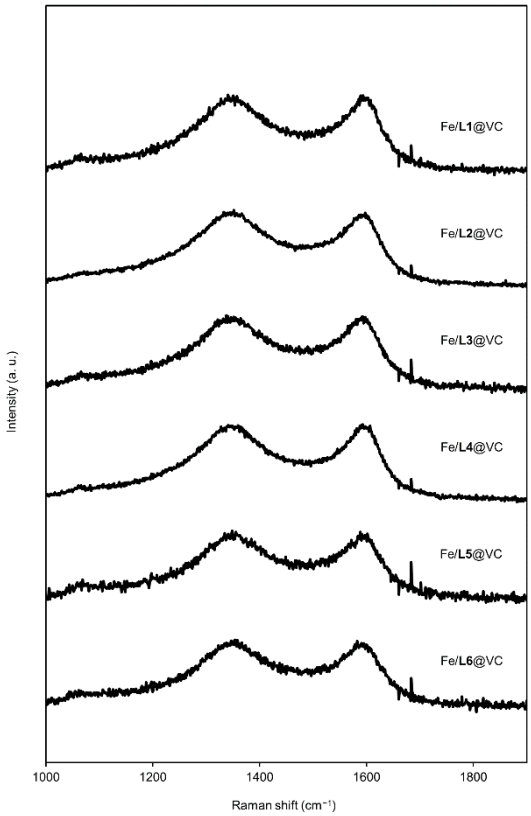

Figure S6. Raman spectra of Fe/**L1**@VC−Fe/**L6**@VC. I_D/I_G values are determined to be 1.07 (Fe/**L1**@VC), 1.07 (Fe/**L2**@VC), 1.07 (Fe/**L3**@VC), 1.14 (Fe/**L4**@VC), 1.12 (Fe/**L5**@VC), and 1.05 (Fe/**L6**@VC).

Electron microscopic observations

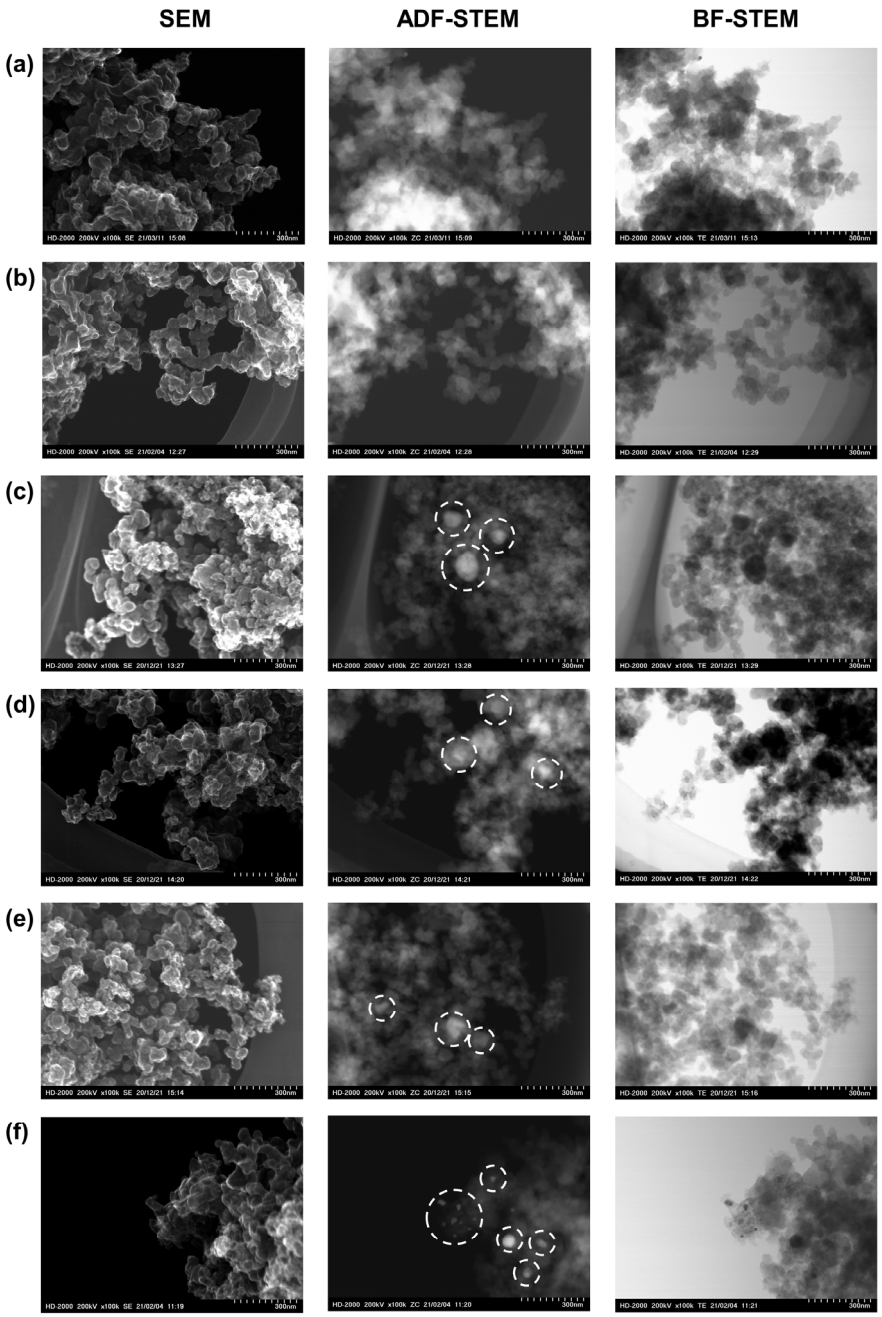

Figure S7. SEM, ADF-STEM and BF-STEM images of (a) Fe/**L1**@VC, (b) Fe/**L2**@VC, (c) Fe/**L3**@VC, (d) Fe/**L4**@VC, (e) Fe/**L5**@VC, and (f) Fe/**L6**@VC. Iron aggregates in ADF-STEM images are highlighted with dashed white circle.

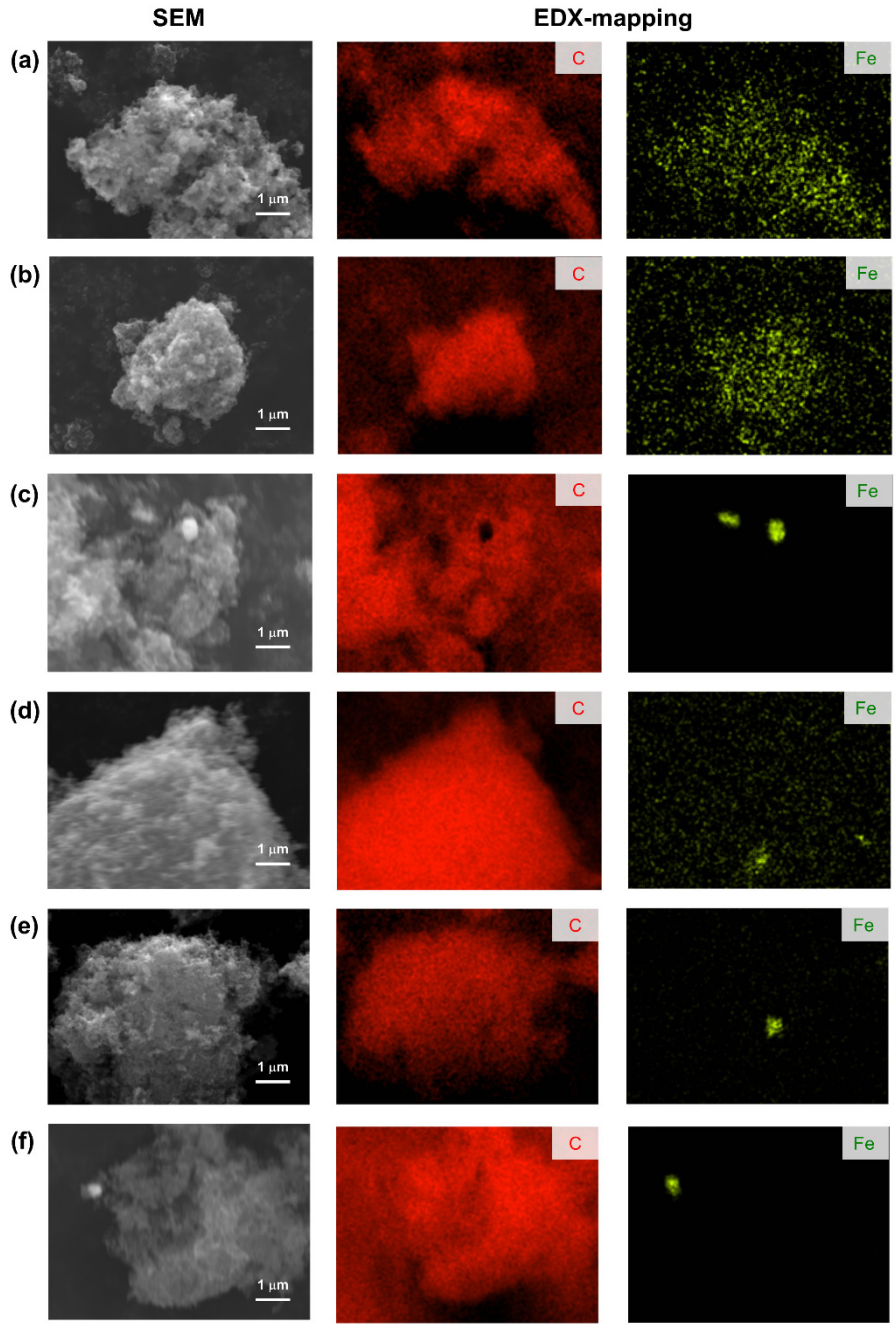

Figure S8. SEM and elemental mapping images of carbon (red) and iron (light green) of (a) Fe/**L1**@VC, (b) Fe/**L2**@VC, (c) Fe/**L3**@VC, (d) Fe/**L4**@VC, (e) Fe/**L5**@VC, and (f) Fe/**L6**@VC.

Elemental analysis

Table S2. Summary of Elemental Analysis for the Fe/N/C Catalysts.

Fe/N/C catalysts	C (wt%)	H (wt%)	N (wt%)	Fe[a] (wt%)	Remained Fe (%)[a,b]
Fe/**L1**@VC	85.34	0.44	1.40	1.35	93
Fe/**L2**@VC	85.61	0.31	1.73	1.66	90
Fe/**L3**@VC	92.16	0	1.10	1.45	52
Fe/**L4**@VC	89.79	0.5	1.28	1.65	67
Fe/**L5**@VC	92.46	0	0.62	1.88	59
Fe/**L6**@VC	95.69	0.13	0.38	1.76	62

[a] Determined by ICP-OES. [b] The percentage of iron content in the Fe/N/C catalyst relative to the amount of iron in the precursor (0.05 mmol).

BET specific surface areas

Table S3. Summary of BET Specific Surface Areas.

Fe/N/C catalysts	BET specific surface area ($m^2 \cdot g^{-1}$)
Fe/**L1**@VC	328
Fe/**L2**@VC	304
Fe/**L3**@VC	121
Fe/**L4**@VC	155
Fe/**L5**@VC	128
Fe/**L6**@VC	108

X-ray photoelectron spectrometric (XPS) analysis

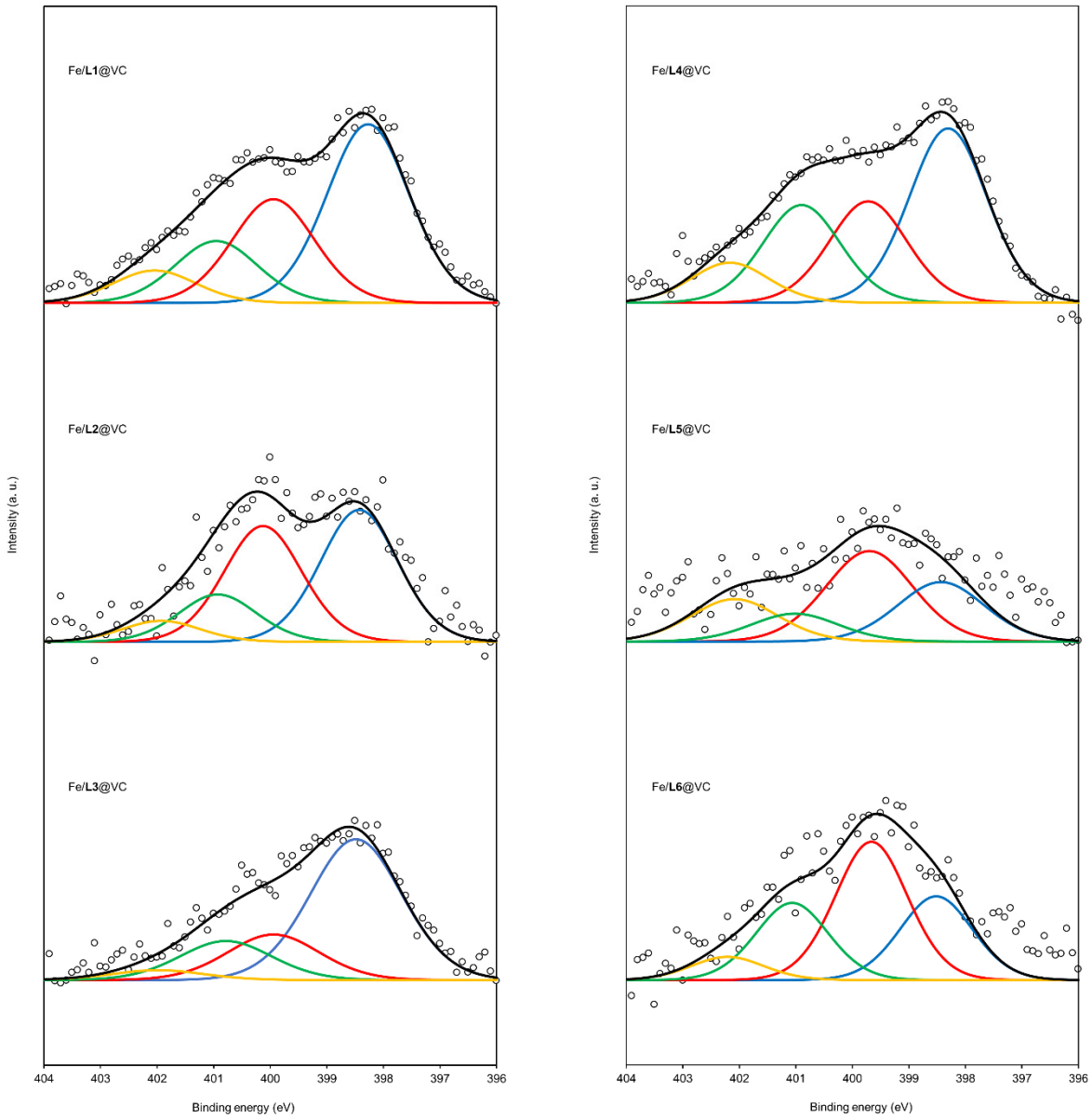

Figure S9. XPS N1s spectra of Fe/**L1**@VC−Fe/**L6**@VC (open circle) with the simulated peaks of Fe−*N* (red), pyridinic *N* (blue), graphitic *N* (green), and *N*-oxide (yellow).

Table S4. Summary of the Relative Ratios of the Four Nitrogen Species.

Fe/N/C catalysts	Fe−*N* (%)	Pyridinic *N* (%)	Graphitic *N* (%)	*N*-oxide (%)
Fe/**L1**@VC	28	47	16	9
Fe/**L2**@VC	37	42	15	7
Fe/**L3**@VC	19	60	17	4
Fe/**L4**@VC	24	42	25	10
Fe/**L5**@VC	41	27	13	19
Fe/**L6**@VC	43	26	24	7

Table S5. Summary of the Amounts of the Four Nitrogen Species.

Fe/N/C catalysts	Fe−*N* (wt%)	Pyridinic *N* (wt%)	Graphitic *N* (wt%)	*N*-oxide (wt%)
Fe/**L1**@VC	0.39	0.66	0.23	0.12
Fe/**L2**@VC	0.63	0.72	0.26	0.12
Fe/**L3**@VC	0.21	0.66	0.18	0.05
Fe/**L4**@VC	0.31	0.59	0.34	0.13
Fe/**L5**@VC	0.25	0.17	0.08	0.12
Fe/**L6**@VC	0.16	0.10	0.09	0.03

X-ray absorption spectrometric (XAS) analysis

In-situ electrochemical Fe K-edge XAS measurements were carried out at the beamline BL12C, Photon Factory (PF), Institute of Materials Structure Science (IMSS), KEK, Japan. The XAS data were collected at room temperature in the fluorescent mode using a manganese K-edge filter (absorption edge height = 3) and a 7-element silicon drift detector (SDD). A three-electrode electrochemical flow cell was utilized for the *in-situ* XAS experiments.[11] A Pt wire counter electrode and the Ag/AgCl (sat. KCl) reference electrode were used. The potential applying to the working electrode during the measurements were controlled using an Ivium Compactstat potentilstat. All *in situ* XAS measurements were performed in a 0.1 M $HClO_{4aq}$ under N_2. To prepare working electrodes of Fe/**L1**@VC and Fe/**L2**@VC for *in situ* XAS experiments, the catalyst ink containing Fe/N/C catalysts (Fe/**L1**@VC, Fe/**L2**@VC) (4.0 mg) and 5% Nafion 117 dispersion (100 μL) was sonicated for at least 2 h, and then the ink (ca. 50 μL) was drop-cast on a gold film sputtered on a Kapton window. The resulting electrode was heated in an oven at 418 K for 5 min. *In-situ* XAS data were analyzed using software packages REX2000 (Rigaku Co.) or Athena (Demeter 0.9.24). The ratio of Fe^{2+} and Fe^{3+} in each applied voltage was determined by linear combination fitting analysis and the reduction potentials were calculated by Nernst equation:

$$E = E^o + \frac{RT}{nF}\ln\frac{a_{Ox}}{a_{Red}}$$

where E is the electrode potential, E^0 is the standard electrode potential, R is the universal gas constant, T is the temperature, n is the number of electrons transferred in the reaction, F is the Faraday constant, and a is the chemical activity for the relevant species. Extended X-ray absorption fine structure (EXAFS) oscillation values, $\chi(k)$, in the k range from 3 to 12 $Å^{-1}$ were extracted from XAS spectra. The $k^3 \cdot \chi(k)$ values were Fourier-transformed into R-space, followed by the inverse Fourier transform into k-space for curve-fitting using the following equation:

$$\chi(k) = \sum_j \frac{N_j S_0^2 F_j(k)}{k R_j^2} \exp\left[-2k^2\sigma_j^2\right] \exp\left[\frac{-2R_j}{\lambda(k)}\right] \sin\left[2kR_j + \phi_j(k)\right]$$

where S_0^2 is the amplitude reduction factor, $F_j(k)$ is the effective curved-wave backscattering amplitude, N_j is the number of neighbors in the j^{th} atomic shell, R_j is the distance between the X-ray absorbing central atom and the atoms in the j^{th} atomic shell (backscatterer), $\phi_j(k)$ is the phase function (including the phase shift for each shell and the total central atom phase shift), and σ_j is the Debye-Waller parameter of the j^{th} atomic shell (variation of distances around the average R_j). The $\phi_j(k)$, and $F_j(k)$ were calculated using the FEFF8.20 program.[12] For FEFF calculations, a molecular geometry was taken from the single crystal X-ray analysis data of a Fe complex of hexaaza macrocylic (HAM) ligand, $[(H_2O)\{Fe(H_2HAM)\}(\mu\text{-}O)\{Fe(H_2HAM)\}(\mu\text{-}O)\{Fe\text{-}(H_2HAM)\}(OH_2)]Br_6$.[13] The curve-fitting analysis was performed using the REX2000 software package.[14]

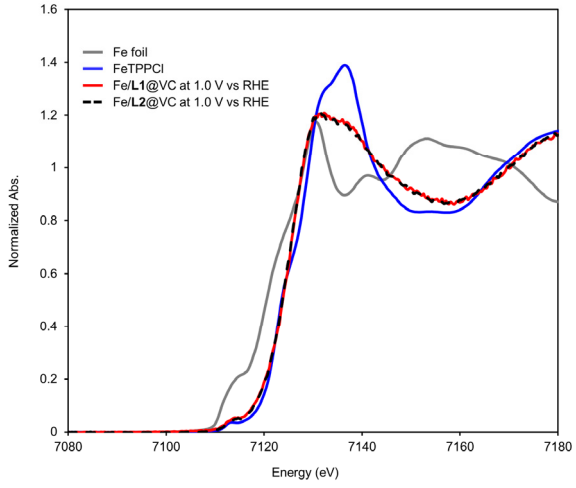

Figure S10. Fe *K*-edge XANES spectra of Fe foil (gray), Fe(III)-tetraphenylporphyrin complex (FeTPPCl) (blue), Fe/**L1**@VC at 1.0 V vs RHE (red), and Fe/**L2**@VC at 1.0 V vs RHE (black dashed line).

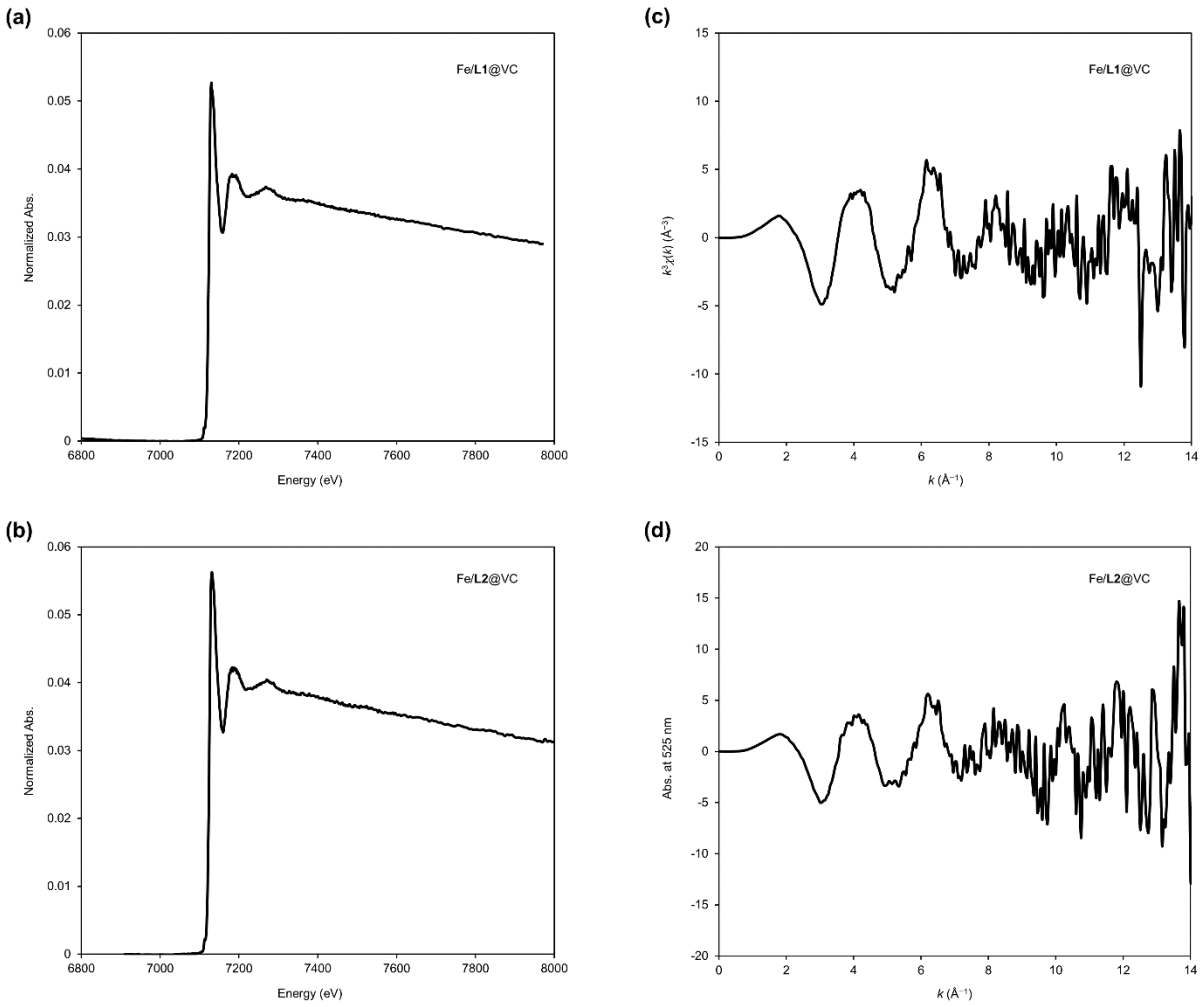

Figure S11. Fe *K*-edge XANES spectra of (a) Fe/**L1**@VC and (b) Fe/**L2**@VC at 1.0 V vs RHE. EXAFS oscillations of (c) Fe/**L1**@VC and (d) Fe/**L2**@VC.

Table S6. Summary of Curve Fitting Analysis for the Fe/N/C Catalysts at 1.0 V vs RHE.

Fe/N/C catalysts	Coordination atom	Coordination number	*R* (Å)	Debye-Waller factor (Å)	*R*-factor (%)
Fe/**L1**@VC	Nitrogen	4.3 ± 0.3	1.99 ± 0.02	0.08 ± 0.01	1.6
Fe/**L2**@VC	Nitrogen	4.1 ± 0.6	1.97 ± 0.02	0.08 ± 0.02	0.8

2.5. Electrochemical Measurements

The setup for the electrochemical measurements using the catalyst ink has been described in our previous reports.[15] The performance of the catalyst in HER was evaluated in a 0.1 M $HClO_{4aq}$ solution. A rotating ring-disk electrode (RRDE) with a glassy carbon disk electrode (ϕ = 5 mm) and platinum ring was used for evaluation of the carbon catalysts. Electrode rotation rates were controlled using a Pine Instruments AFMSRCE rotator with a Pine MSRX motor controller. An electrode was polished to mirror flat with alumina powder (50 nm) before use. The catalyst ink was prepared with 4.0 mg of catalyst and 100 μL of 5 wt% Nafion® (Sigma–Aldrich) in a mixture of lower aliphatic alcohols and H_2O. The ink was vortexed and sonicated in an ultrasonic bath at 100 W at 35 kHz for 30 min. Then, 2 μL of catalyst ink was loaded onto the surface of the electrode and dried. Electrochemical tests were conducted with a potentiostat (ALS, electrochemical analyzer model 610B using a typical three-electrode system, with platinum wire as a counter electrode and Ag/AgCl as a reference electrode. The potential difference between Ag/AgCl and RHE was calculated, and the value is 0.258 V in a 0.1 M $HClO_{4aq}$ solution. The scan rates for all measurements were 5 $mV{\cdot}s^{-1}$ from −0.258 to 0.842 V versus the Ag/AgCl reference electrode. Before each potential scan, the electrolyte of the 0.1 M $HClO_{4aq}$ solution was saturated with O_2 for at least 30 min, and O_2 purging was continued during the electrochemical experiments. The measured currents of disk and ring electrodes were subtracted from the background current at the N_2-saturated electrolyte. In the RRDE test, the ring potential was set to 1.0 V versus the Ag/AgCl reference electrode. The onset potentials (E_{onset}) are defined as a potential showing j = −0.05 $mA{\cdot}cm^{-2}$ in RDE measurement, where j represents the current density. The RRDE collection efficiency (N) was calibrated in 0.1 M $HClO_{4aq}$ with 10 mM $K_3Fe(CN)_6$ electrolyte. The measured N value is 0.26 in our system. The ratio of H_2O_2 in total amount of the product was calculated by equation 1:

$$X_{H2O2} = 2\, I_r / (N \times |I_d| + I_r) \quad \text{---------- (1)}$$

The TOF value which is defined as the number of electrons transferred per an active site and unit time (second) ($e{\cdot}site^{-1}{\cdot}s^{-1}$) was calculated by equation 2:

$$TOF = J_{kin}(0.8\ V\ vs.\ RHE) / (MSD \times e) \quad \text{---------- (2)}$$

where J_{kin} (0.8 V vs. RHE) represents the gravimetric kinetic current density ($A{\cdot}g^{-1}$) at 0.8 V vs RHE, MSD (mass-based site density) is the number of the Fe–N_x active sites normalized by mass of the catalyst ($sites{\cdot}g^{-1}$), and e is elementary charge. The J_{kin} value is calculated by equation 3:

$$J_{kin}\,(0.8\ V\ vs.\ RHE) = J_{lim} \times J_{0.8\,V} / (|J_{lim}| - |J_{0.8\,V}|) \quad \text{---------- (3)}$$

where J_{lim} represents the gravimetric limiting current density, and $J_{0.8\,V}$ is the gravimetric current density observed at 0.8 V vs. RHE. J_{lim} and $J_{0.8\,V}$ can be evaluated from the linear sweep voltammograms in the RDE measurement. MSD was elucidated by CV in an N_2-saturated 0.1 M $HClO_{4aq}$ solution at 10 $mV{\cdot}s^{-1}$ at 2000 rpm from −0.258 to 0.742 V versus the Ag/AgCl reference electrode (Figure S13) and calculated by equation 4:

$$MSD = Q / (e \times n \times g_{cat}) \quad \text{---------- (4)}$$

where Q represents $Fe^{2+/3+}$ coulombic charge (C) calculated by the CV in an N_2-saturated solution, n is reaction number (n = 1 in this redox system), and g_{cat} is loaded weight of the catalyst (0.08 mg). C_{dl} was evaluated by CV in an N_2-saturated 0.1 M $HClO_{4aq}$ solution at difference scan rates (20 $mV{\cdot}s^{-1}$, 40 $mV{\cdot}s^{-1}$, 60 $mV{\cdot}s^{-1}$, 80 $mV{\cdot}s^{-1}$, and 100 $mV{\cdot}s^{-1}$) from 0 to 0.6 V versus RHE (Figure S14).

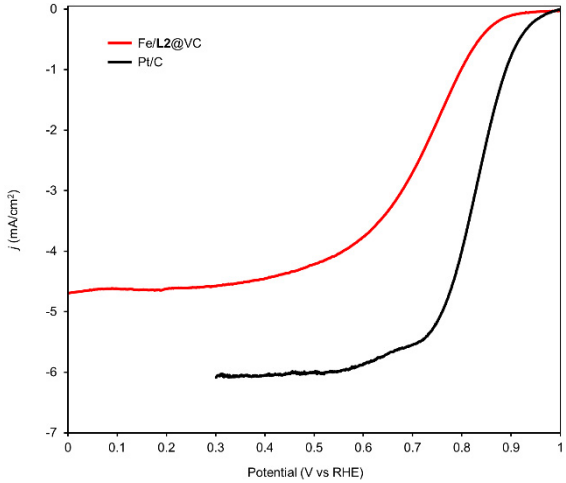

Figure S12. ORR polarization curves of Fe/**L2**@VC (red) and a commercially available Pt/C catalyst (TEC10V30E) (black) in an O_2-saturated 0.1 M $HClO_{4aq}$ solution at 5 mV·s^{-1} at 2000 rpm for the catalysts.

The long-term durabilities of Fe/**L1**@VC and Fe/L**2**@VC were tested by measuring the LSV curve before and after cycling the potential between 0 and 1.0 V vs RHE up to 1000 times (Figure S12). The half-wave potentials ($E_{1/2}$) showed negative shifts of 31 mV (Fe/**L1**@VC) and 25 mV (Fe/**L2**@VC) after the cycling.

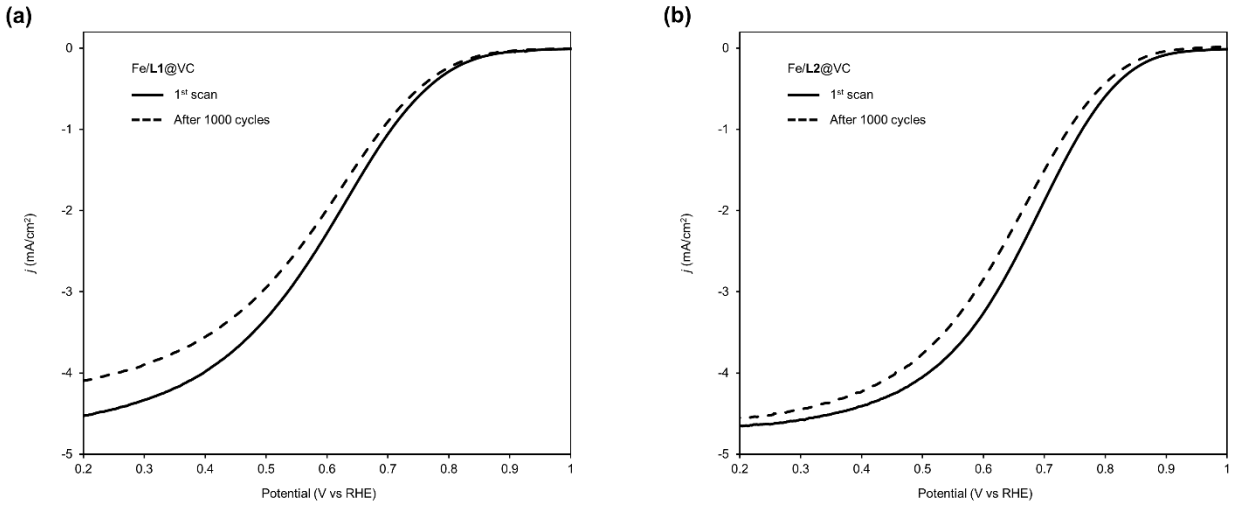

Figure S13. ORR polarization curves of (a) Fe/**L1**@VC and (b) Fe/**L2**@VC before (black solid line) and after (black dashed line) 1000 cycles in an O_2- saturated 0.1 M $HClO_{4aq}$ solution at 5 mV·s^{-1} at 2000 rpm. The potential was cycled between 0 and 1.0 V vs RHE at 50 mV·s^{-1} up to 1000 times in an O_2-saturated 0.1 M $HClO_{4aq}$ solution.

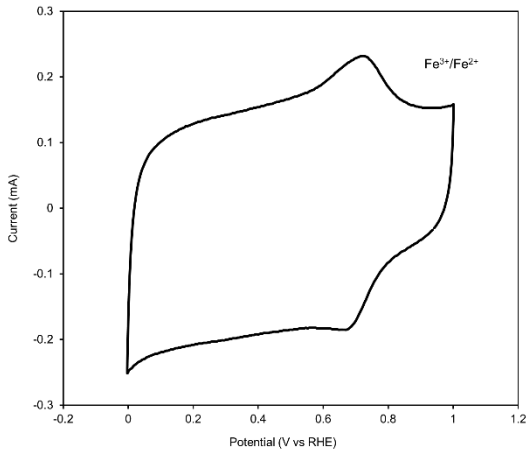

Figure S14. CV curve of Fe/**L2**@VC in an N_2-saturated 0.1 M $HClO_{4aq}$ solution at 50 mV·s^{-1} at 2000 rpm from −0.258 to 0.742 V versus the Ag/AgCl reference electrode.

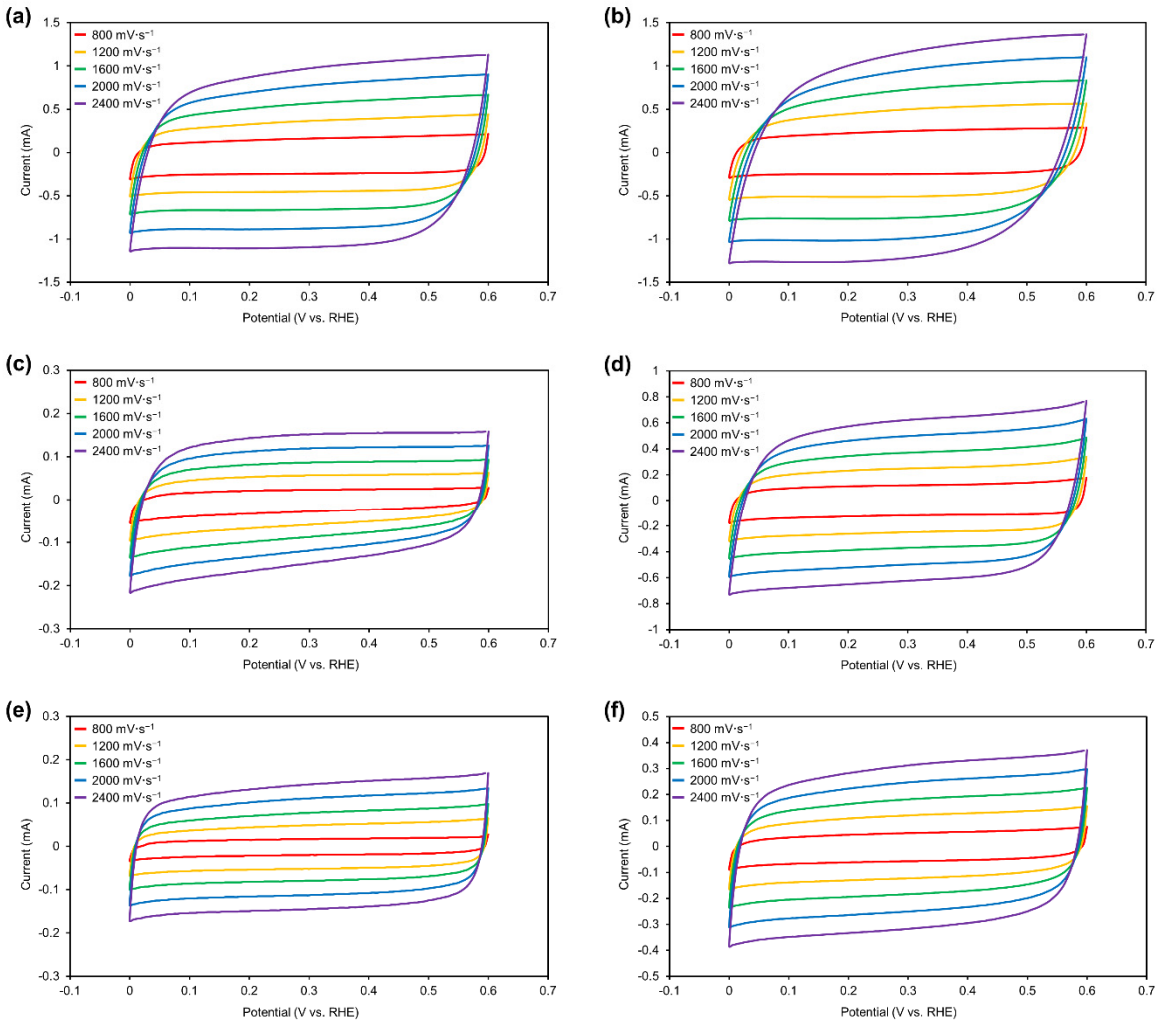

Figure S15. CV curves in an N_2-saturated 0.1 M $HClO_{4aq}$ solution at different scan rate (20 mV·s^{-1}, 40 mV·s^{-1}, 60 mV·s^{-1}, 80 mV·s^{-1}, and 100 mV·s^{-1}) for (a) Fe/L**1**@VC, (b) Fe/L**2**@VC, (c) Fe/L**3**@VC, (d) Fe/L**4**@VC, (e) Fe/L**5**@VC, and (f) Fe/L**6**VC. Capacitive currents at 0.3 V were used for calculation of C_{dl}.

Table S7. Summary of the Electrochemical Analysis for the Fe/N/C Catalysts.

Fe/N/C catalysts	E_{onset} (V)	n at 0.6 V	MSD (10^{19}·sites·g_{cat}^{-1})	TOF at 0.8 V ($e \cdot site^{-1} \cdot s^{-1}$)	C_{dl} (μF)
Fe/**L1**@VC	0.90	3.9	1.8	0.17	10.4
Fe/**L2**@VC	0.93	3.9	3.6	0.21	11.8
Fe/**L3**@VC	0.69	3.6	0.2	0.03	3.1
Fe/**L4**@VC	0.86	3.8	2.7	0.04	6.3
Fe/**L5**@VC	0.79	3.8	1.5	0.02	3.1
Fe/**L6**@VC	0.82	3.7	1.9	0.02	3.3

2.6. NMR Spectra

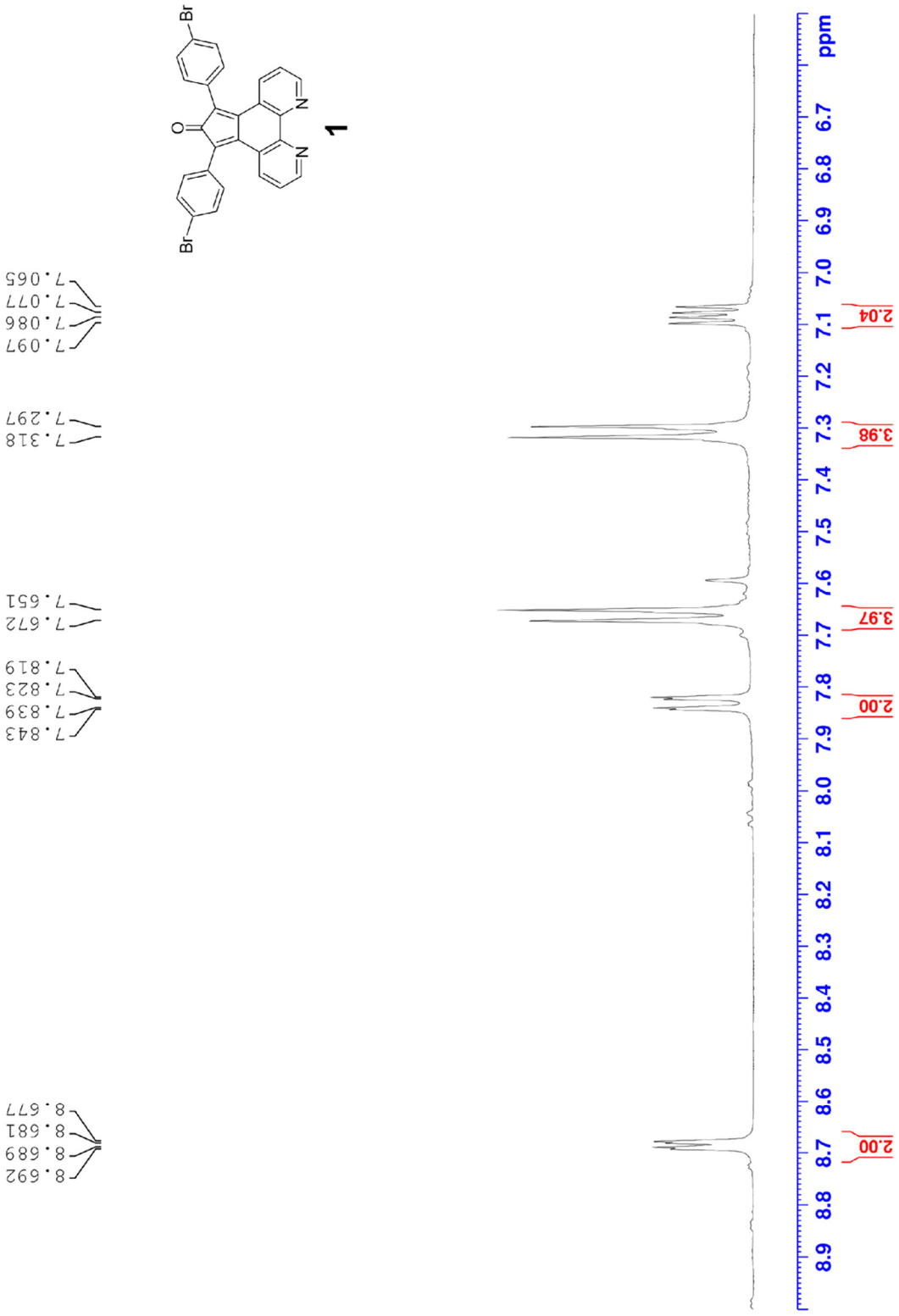

Figure S16. ^{1}H NMR spectrum of **1** (CD_2Cl_2).

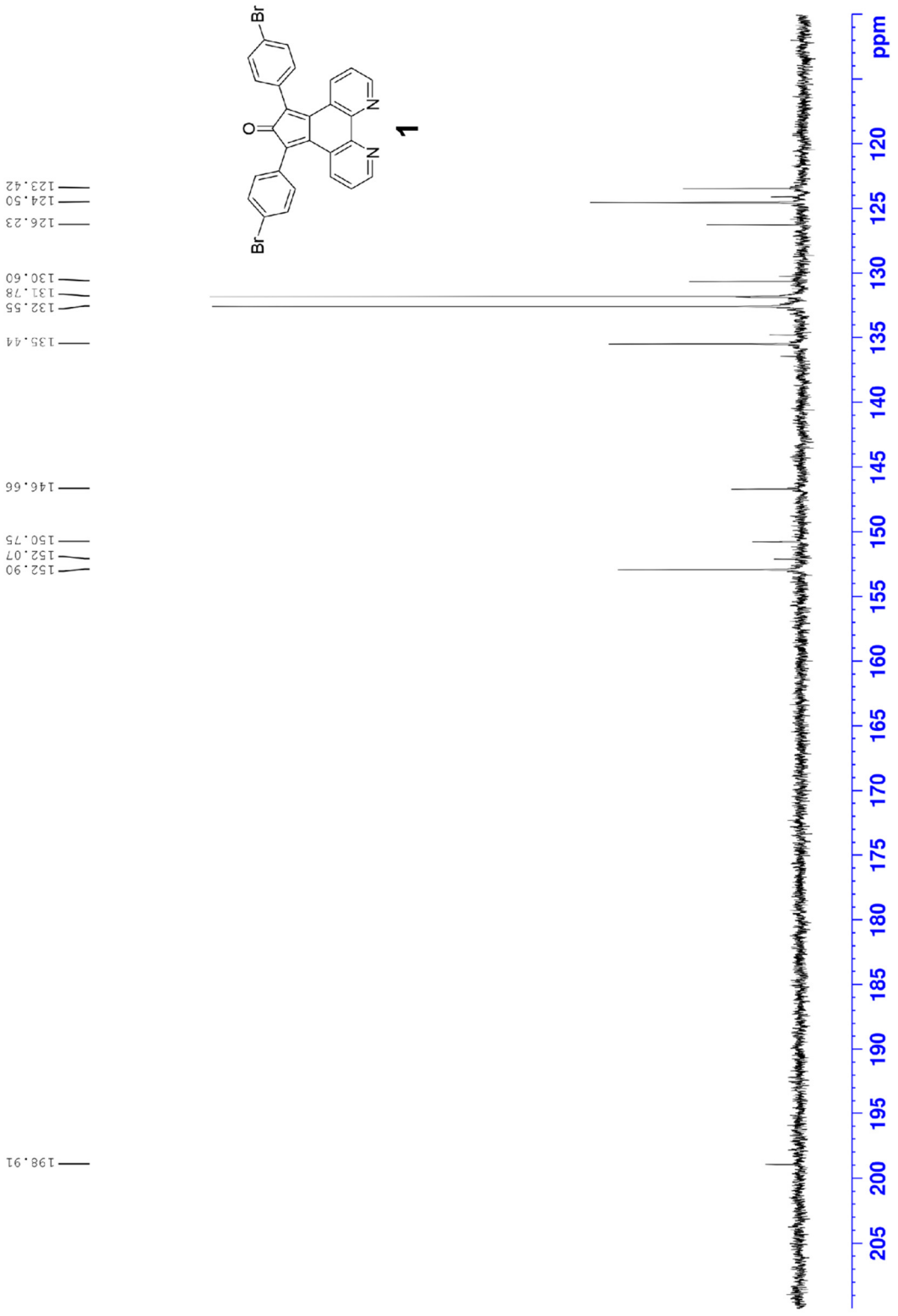

Figure S17. ^{13}C NMR spectrum of **1** (CD_2Cl_2).

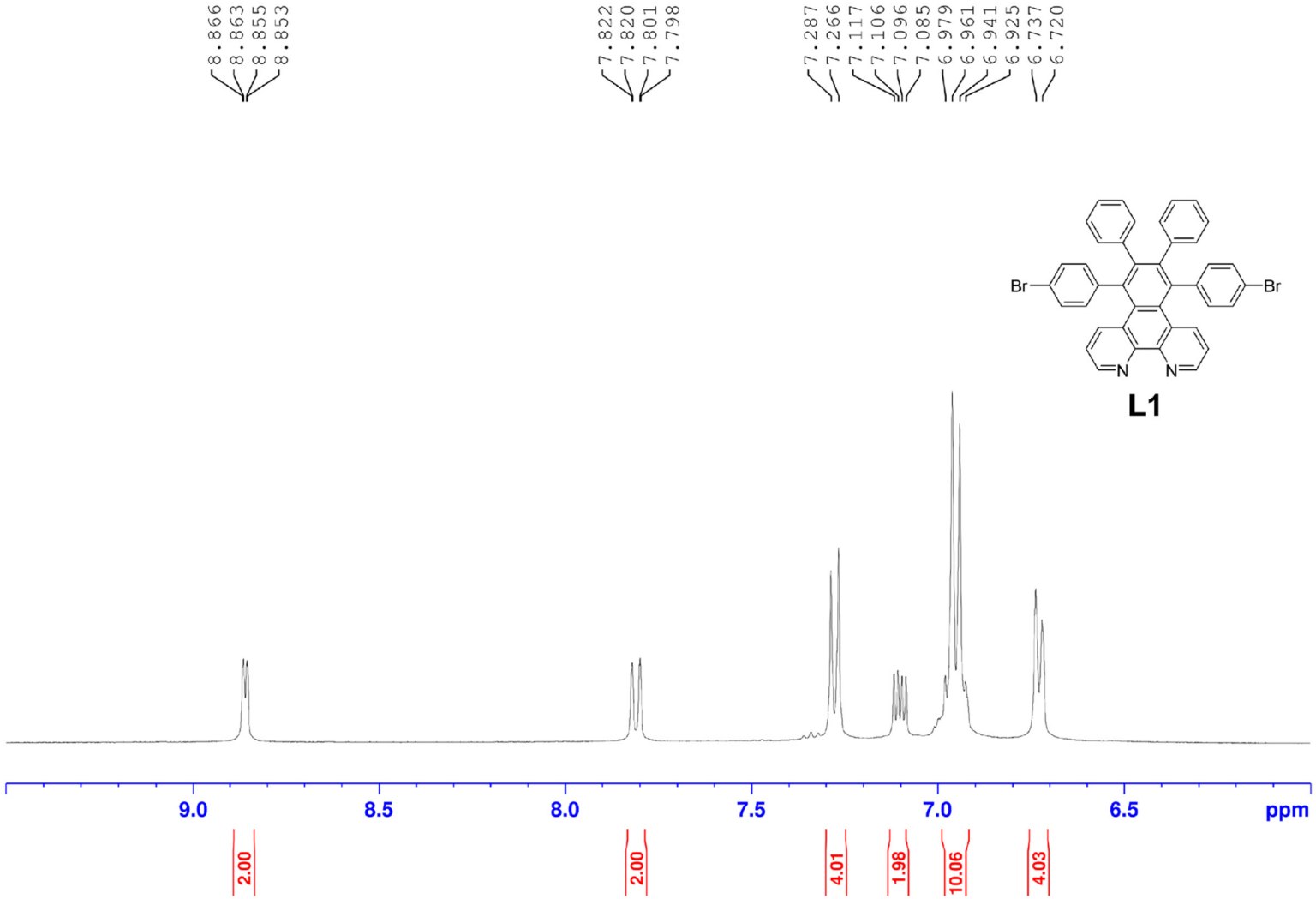

Figure S18. ^{1}H NMR spectrum of **L1** (CD_2Cl_2).

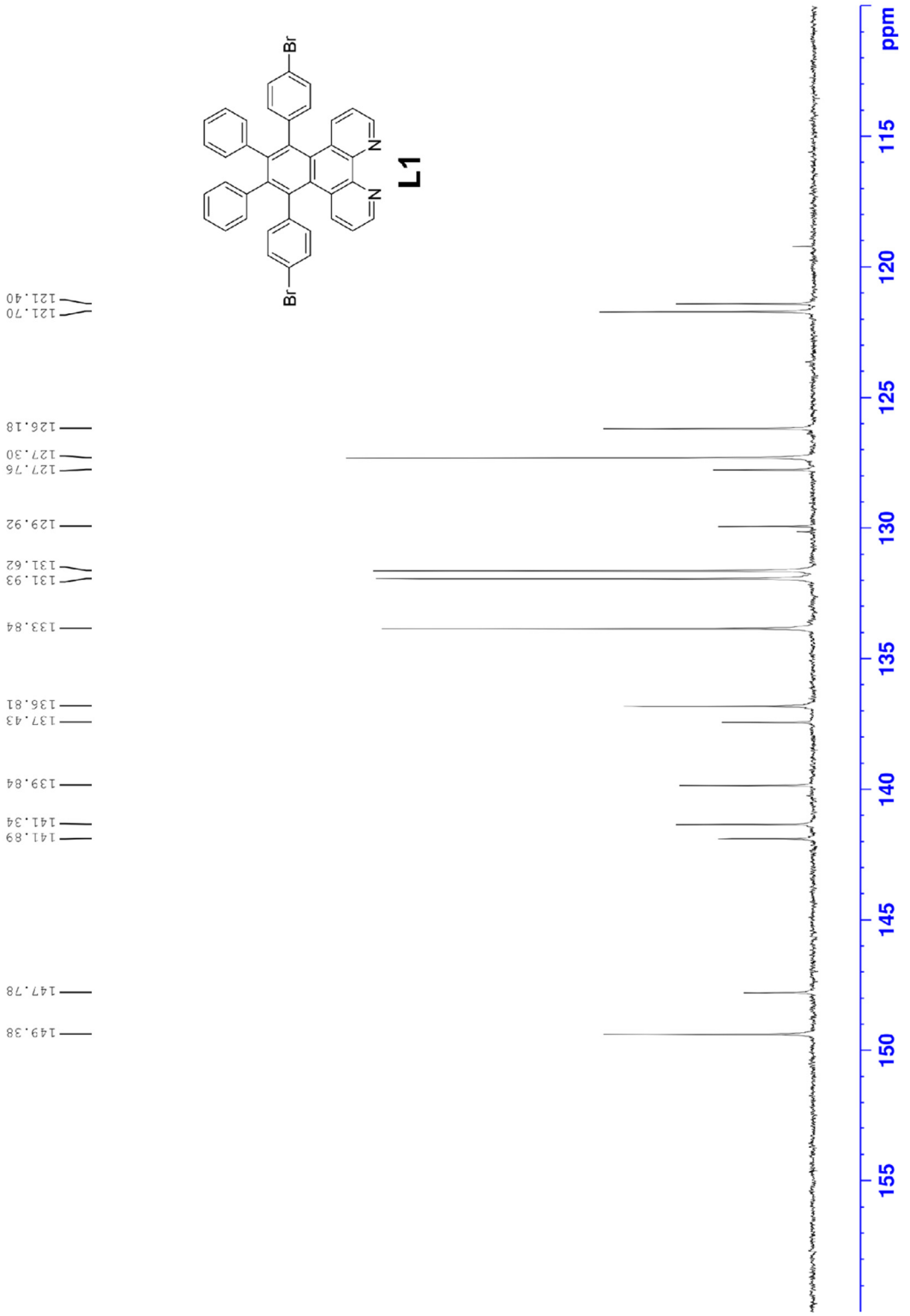

Figure S19. ^{13}C NMR spectrum of **L1** (CD_2Cl_2).

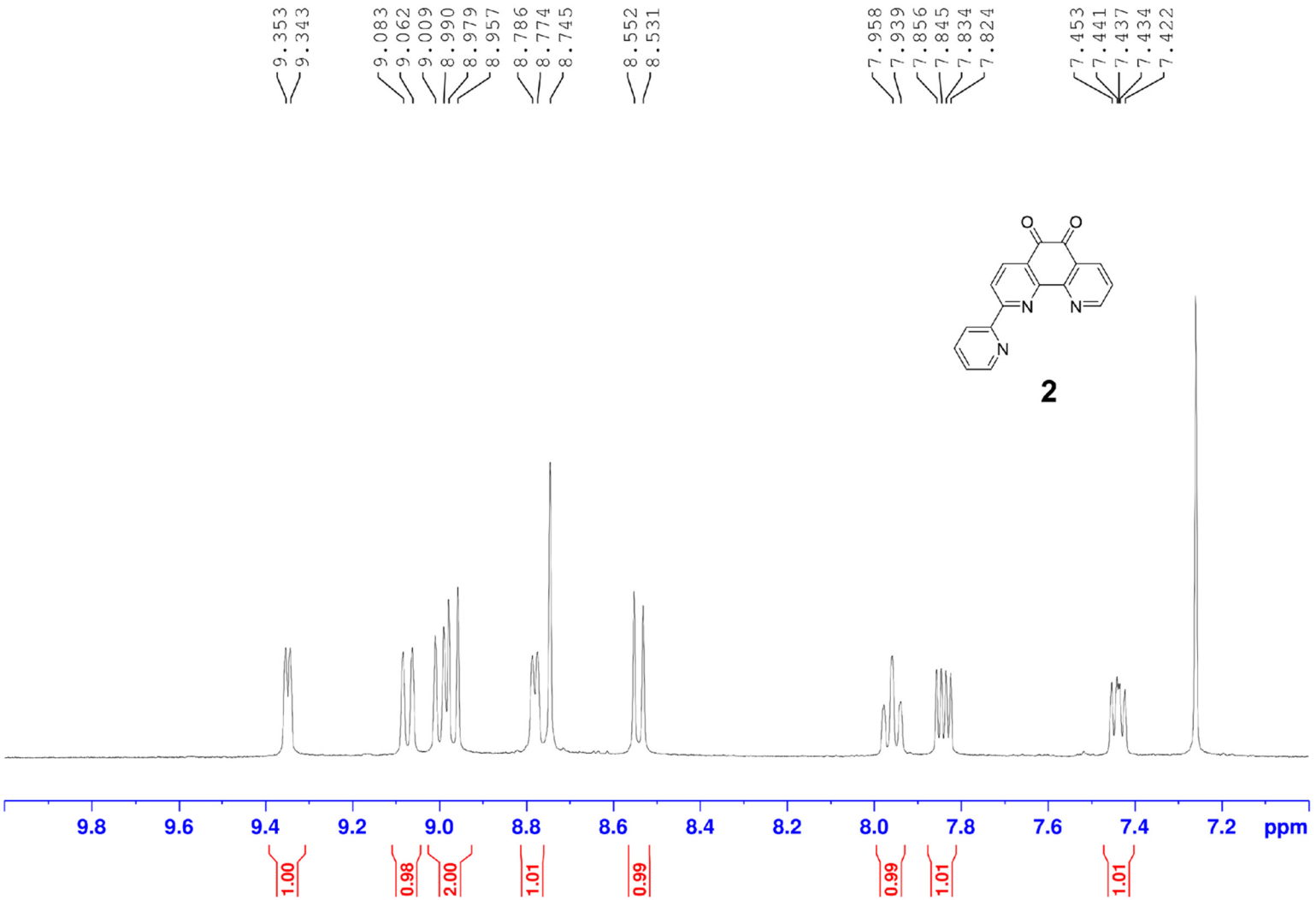

Figure S20. ^{1}H NMR spectrum of **2** ($CDCl_3$).

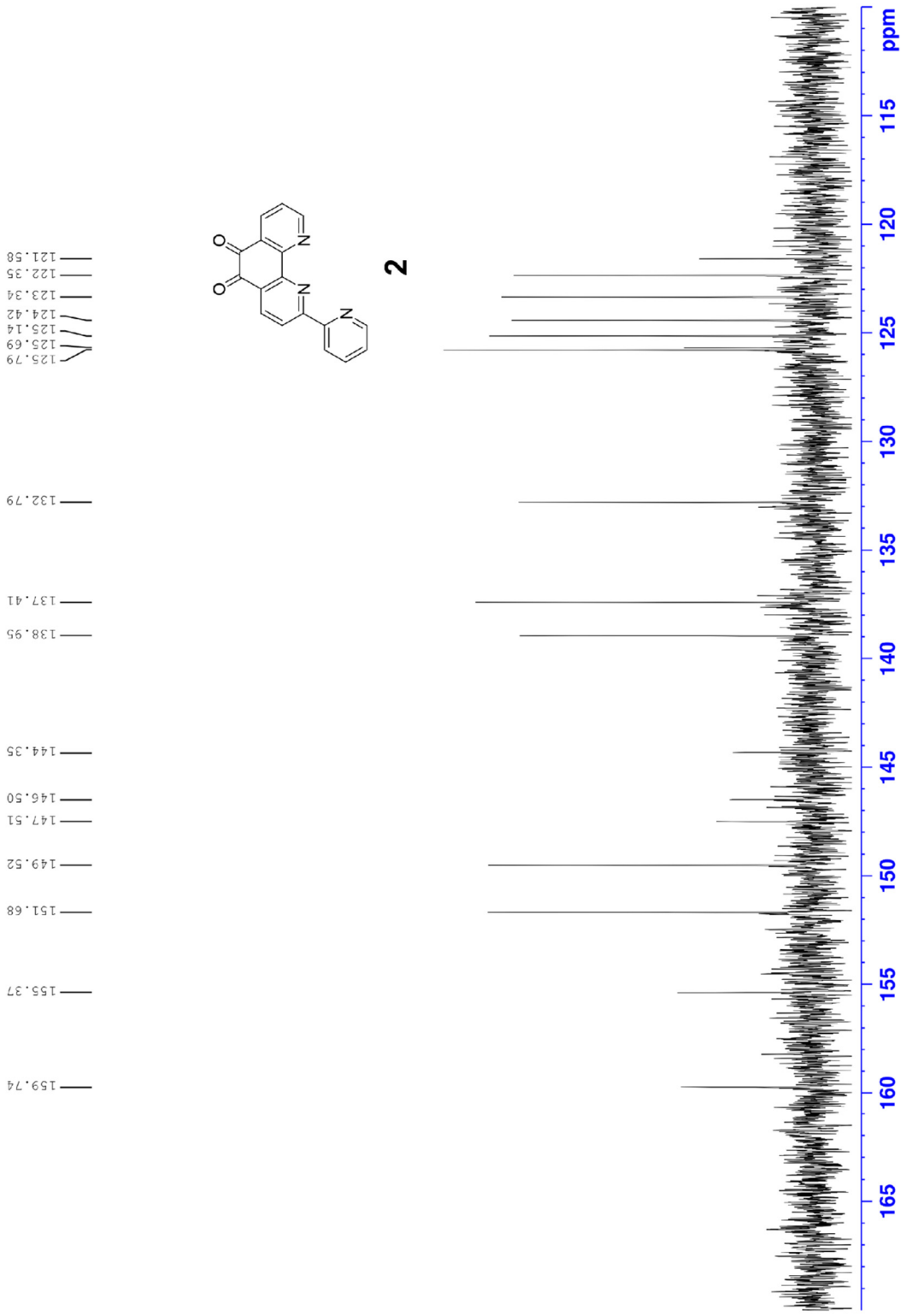

Figure S21. ^{13}C NMR spectrum of **2** ($CDCl_3$).

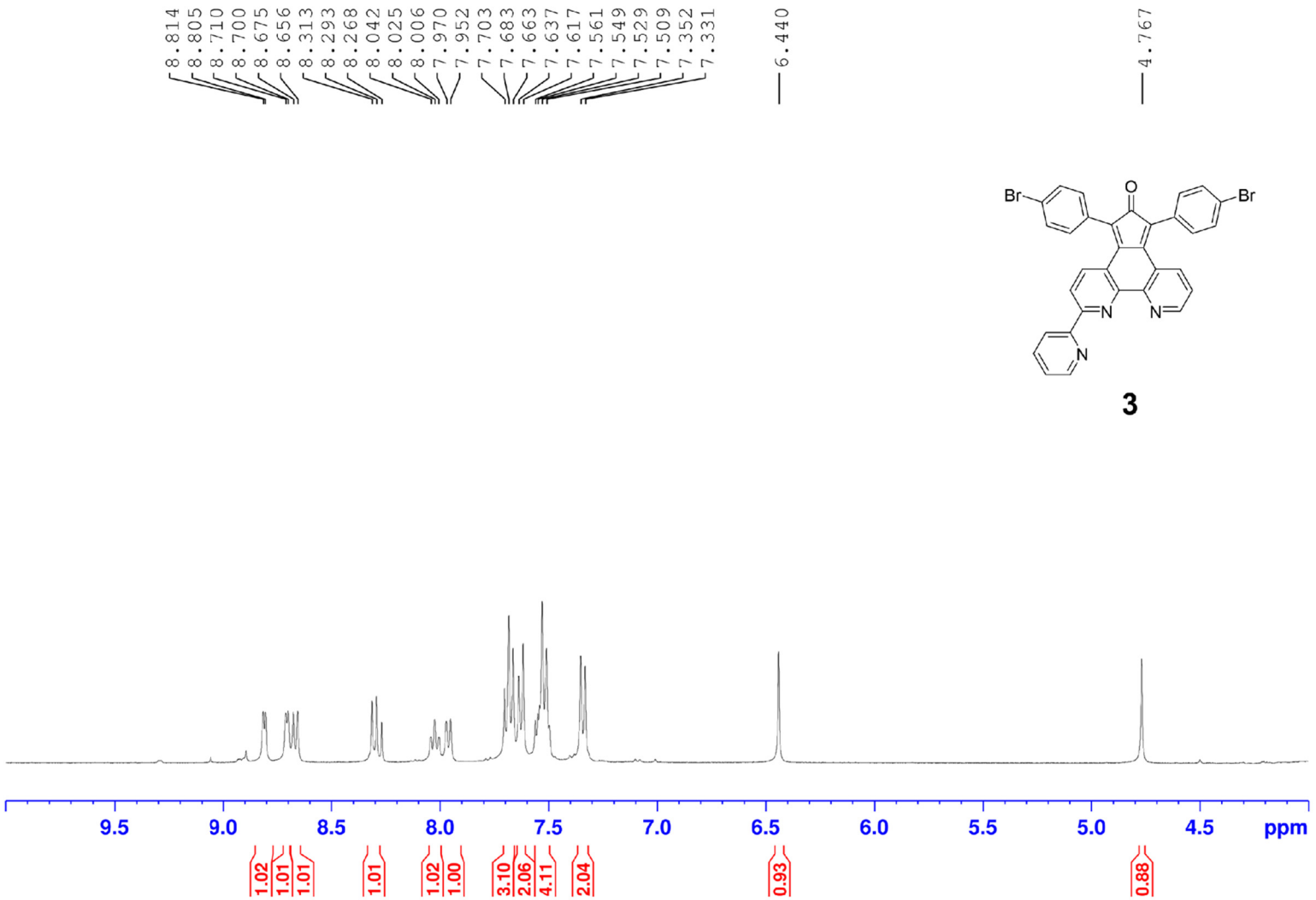

Figure S22. ^{1}H NMR spectrum of **3** (DMSO-d_6).

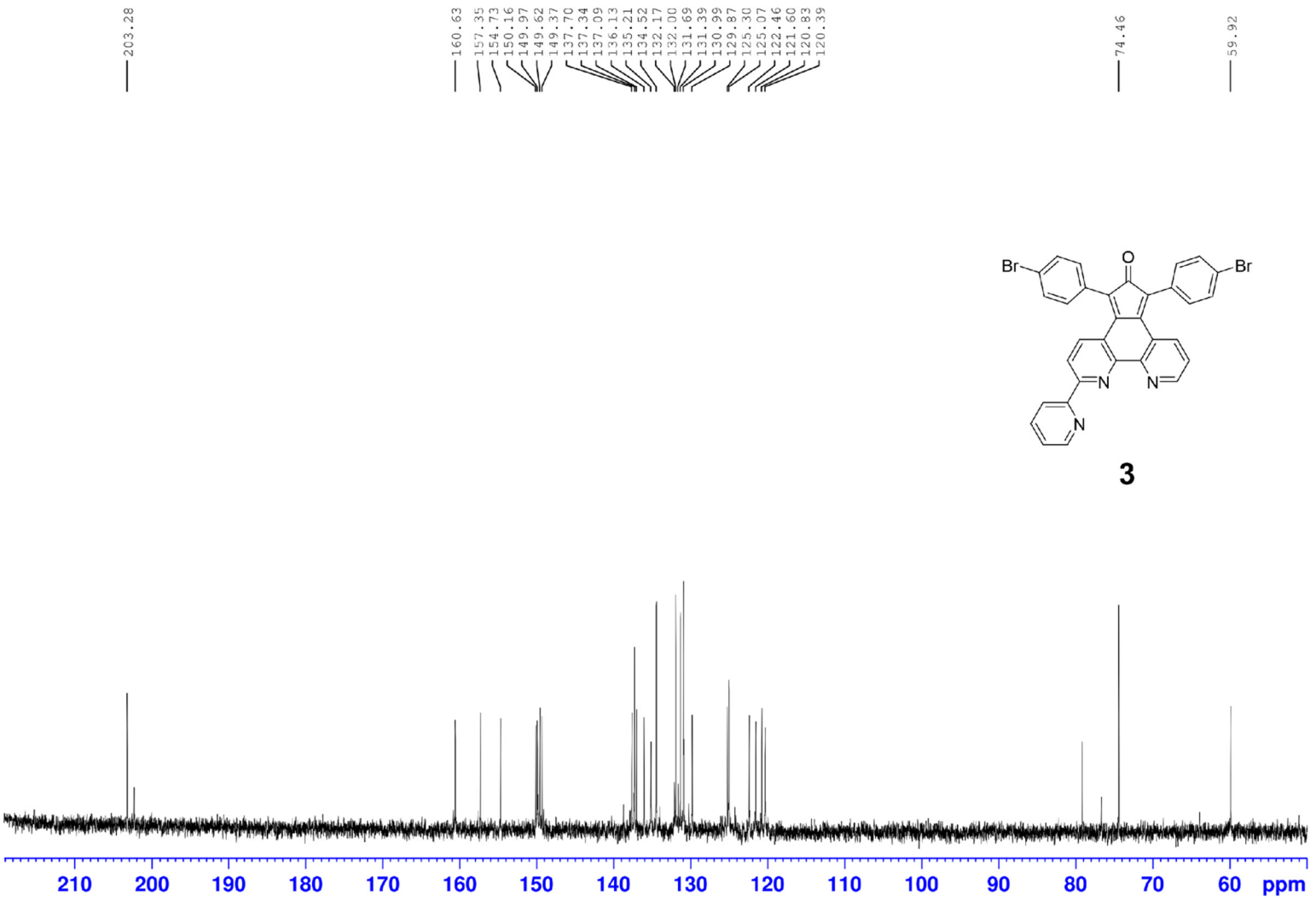

Figure S23. ^{13}C NMR spectrum of **3** (DMSO-d_6).

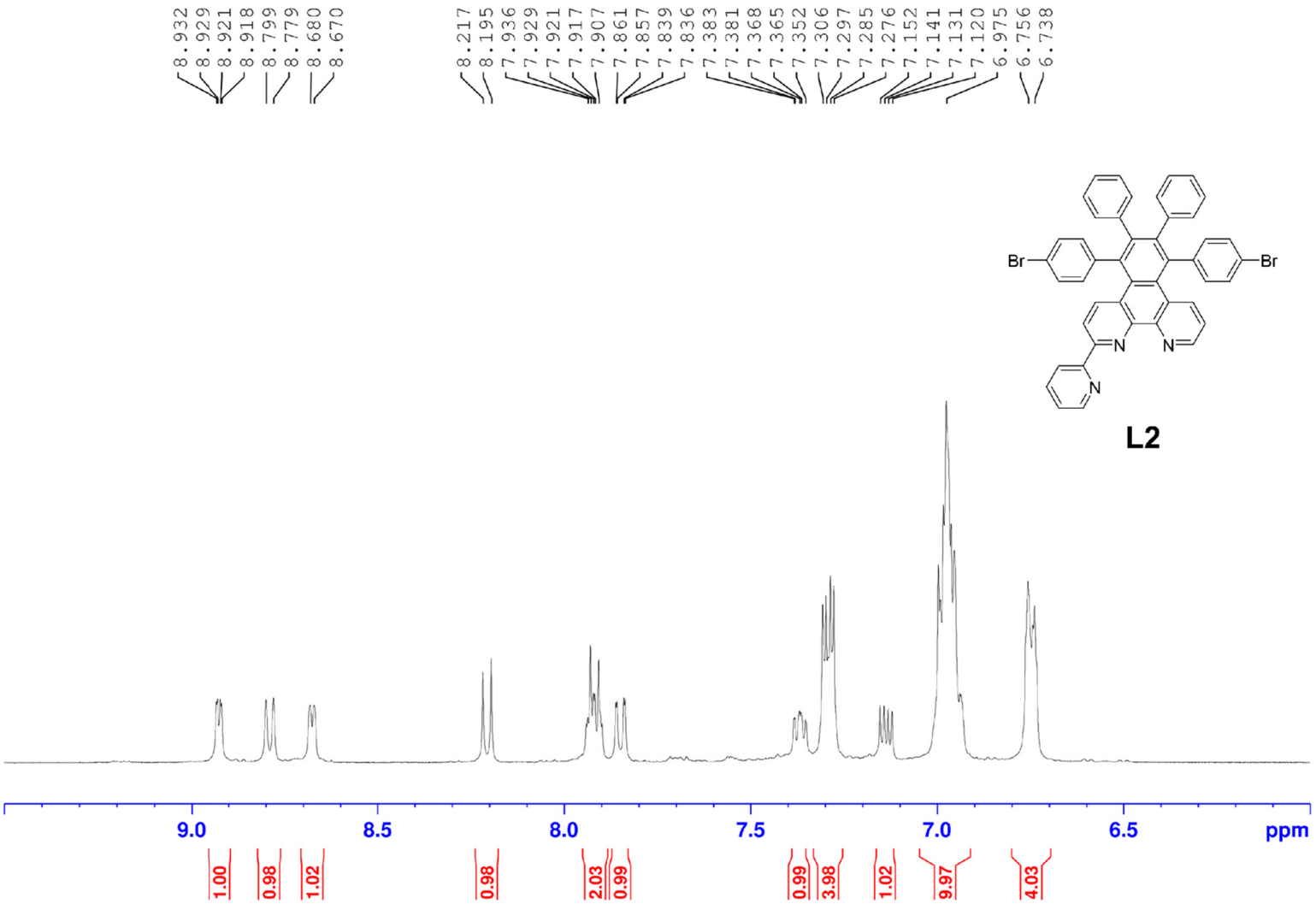

Figure S24. ^{1}H NMR spectrum of **L2** (CD_2Cl_2).

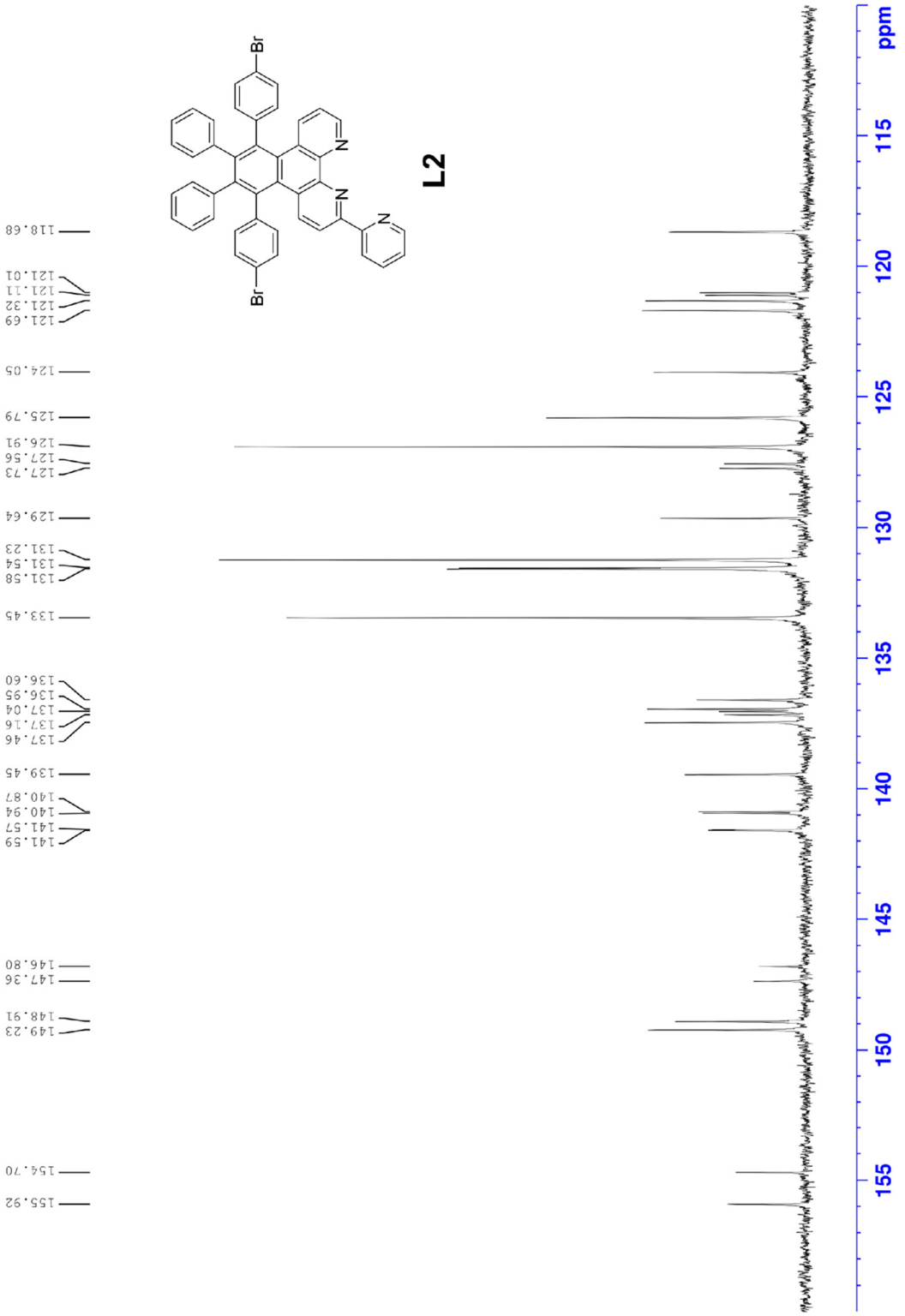

Figure S25. ^{13}C NMR spectrum of **L2** (CD_2Cl_2).

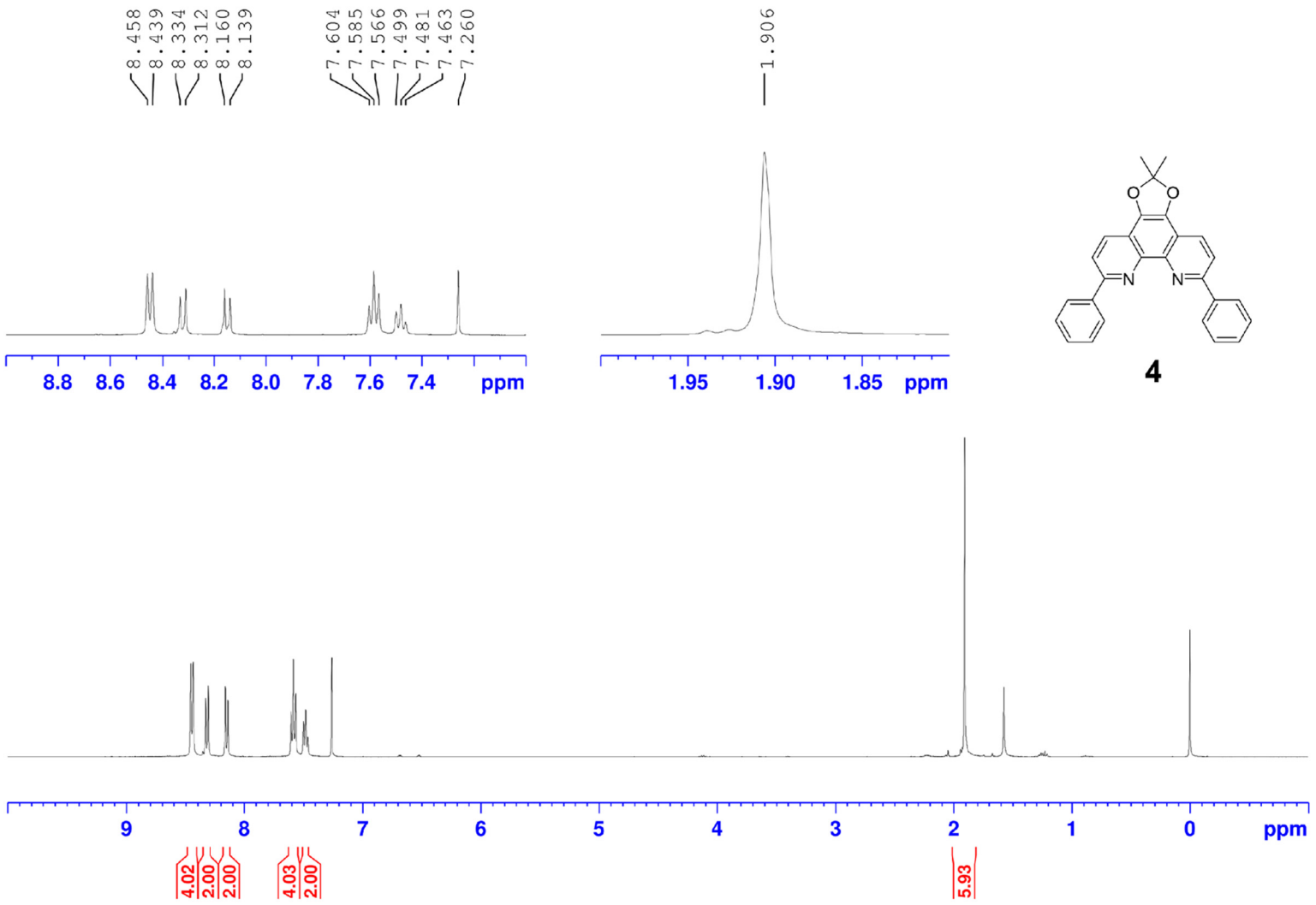

Figure S26. ^{1}H NMR spectrum of **4** ($CDCl_3$).

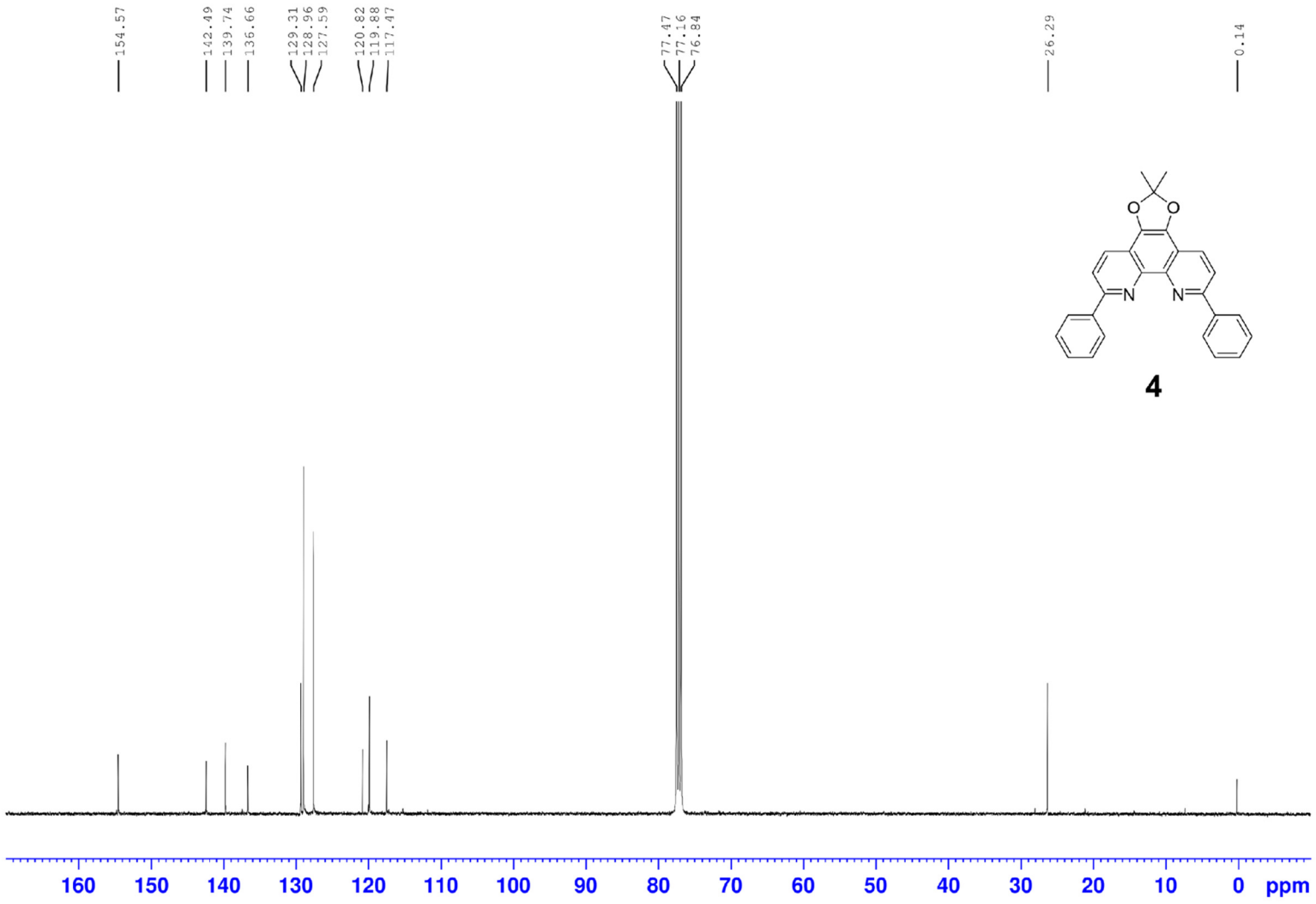

Figure S27. ^{13}C NMR spectrum of **4** ($CDCl_3$).

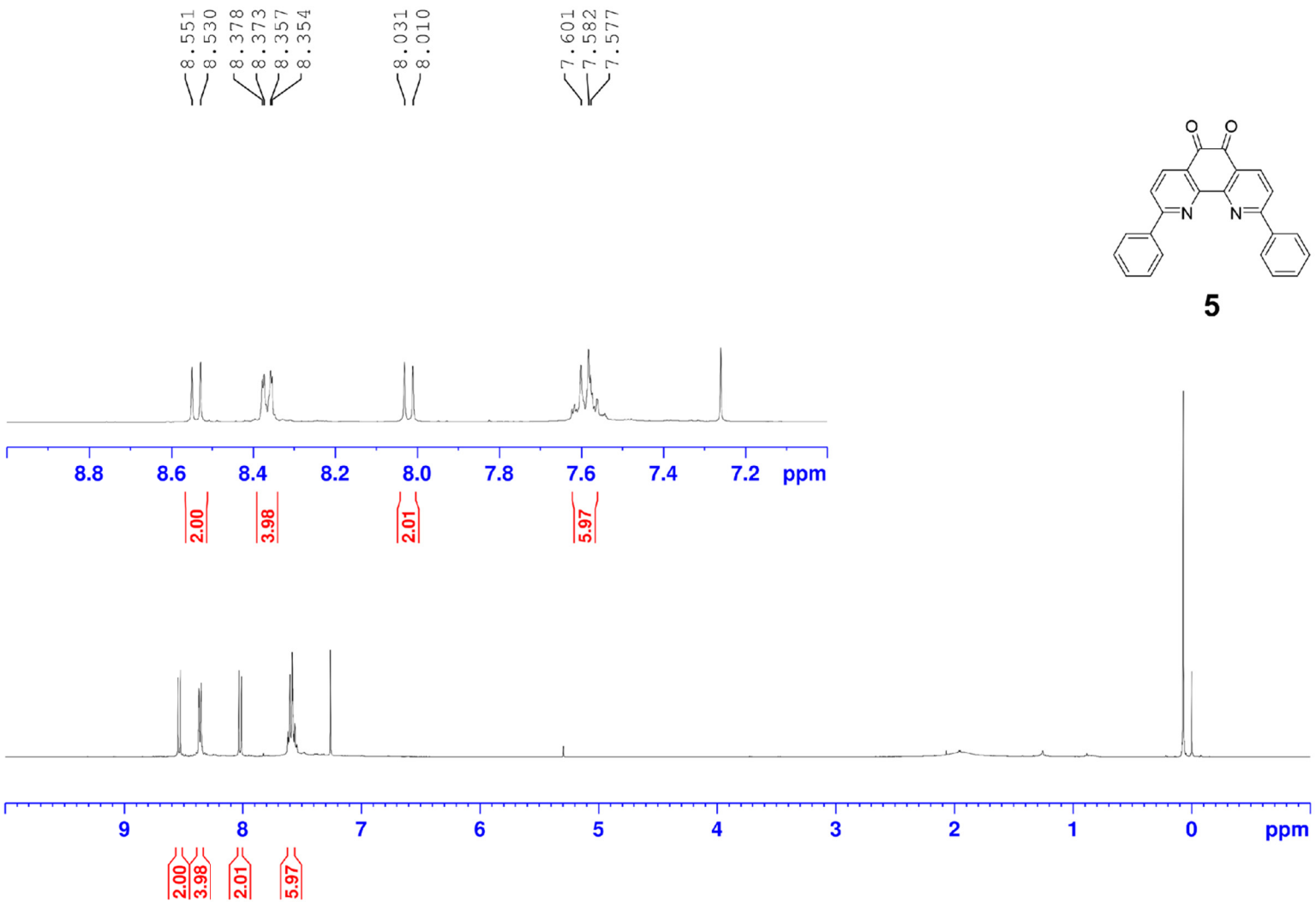

Figure S28. ^{1}H NMR spectrum of **5** ($CDCl_3$).

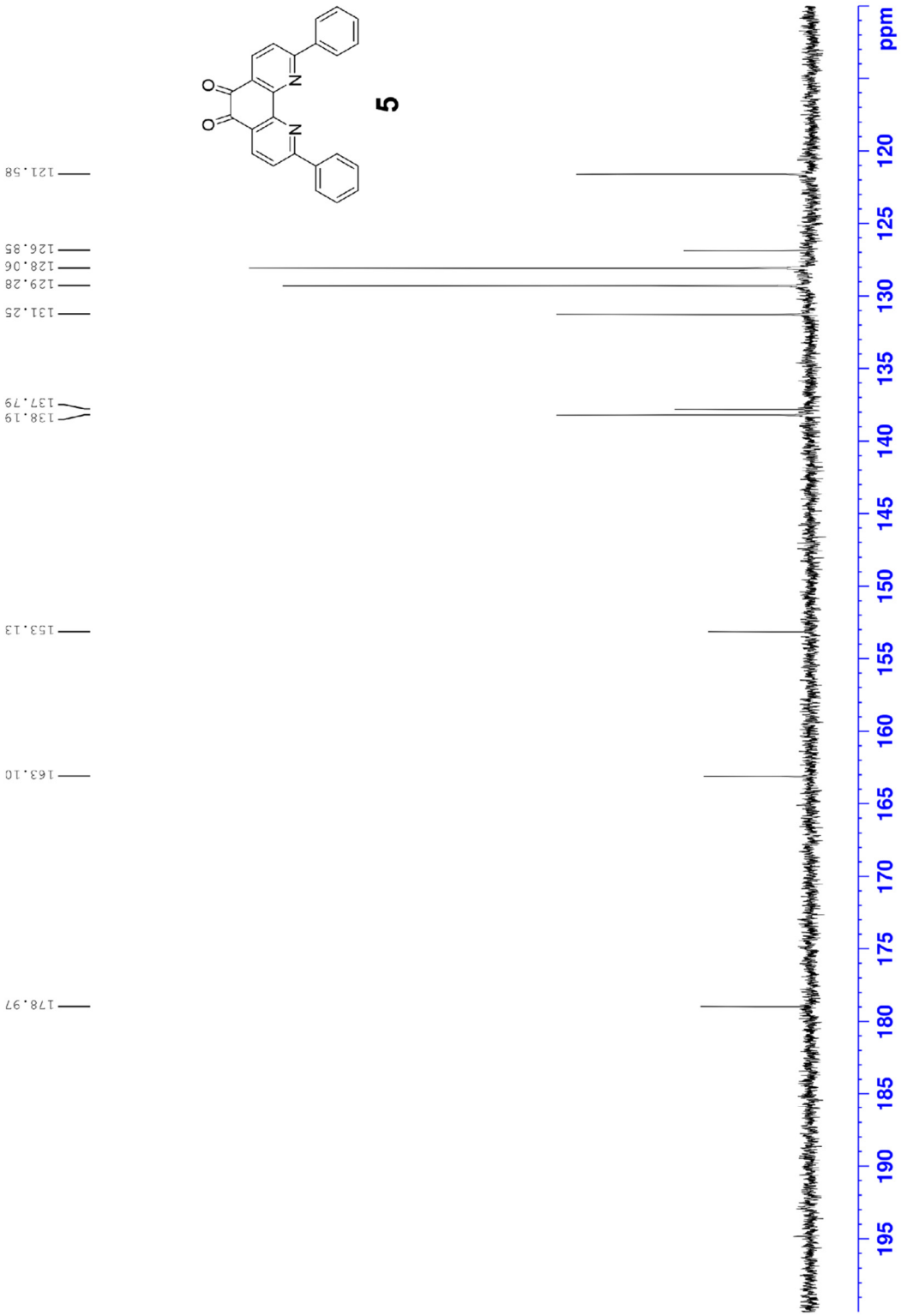

Figure S29. ^{13}C NMR spectrum of **5** ($CDCl_3$).

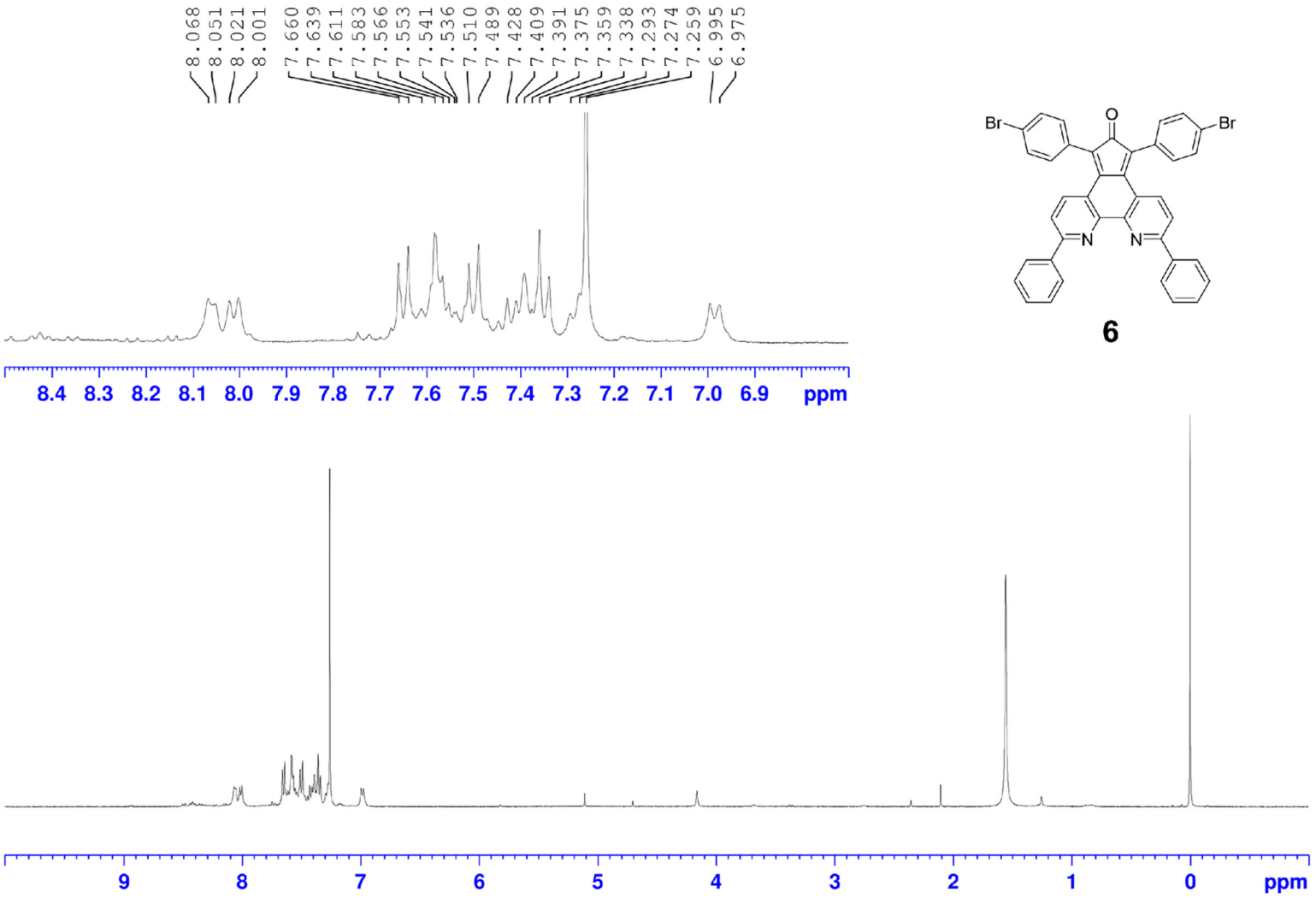

Figure S30. ^{1}H NMR spectrum of **6** ($CDCl_3$).

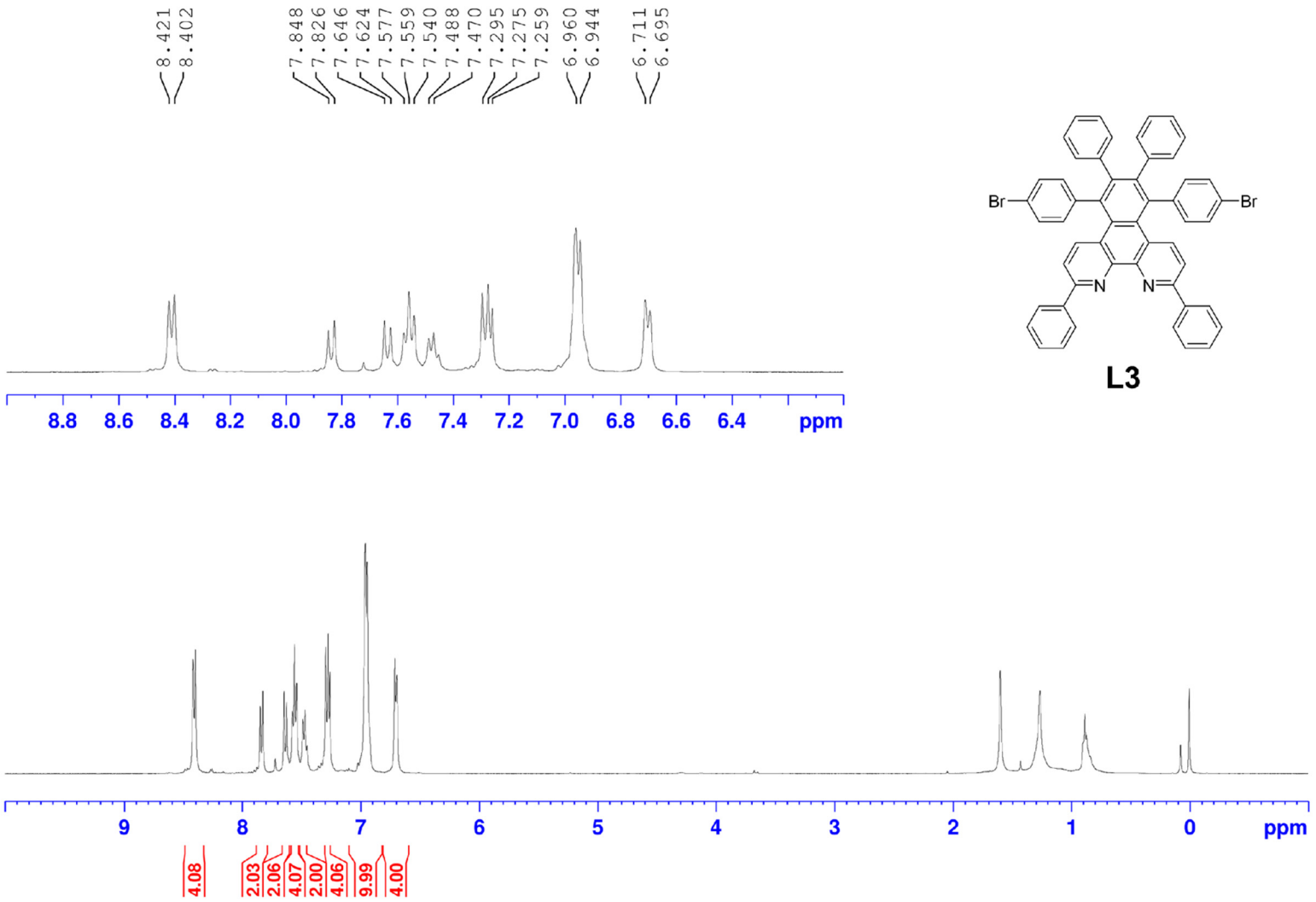

Figure S31. ^{1}H NMR spectrum of **L3** ($CDCl_3$).

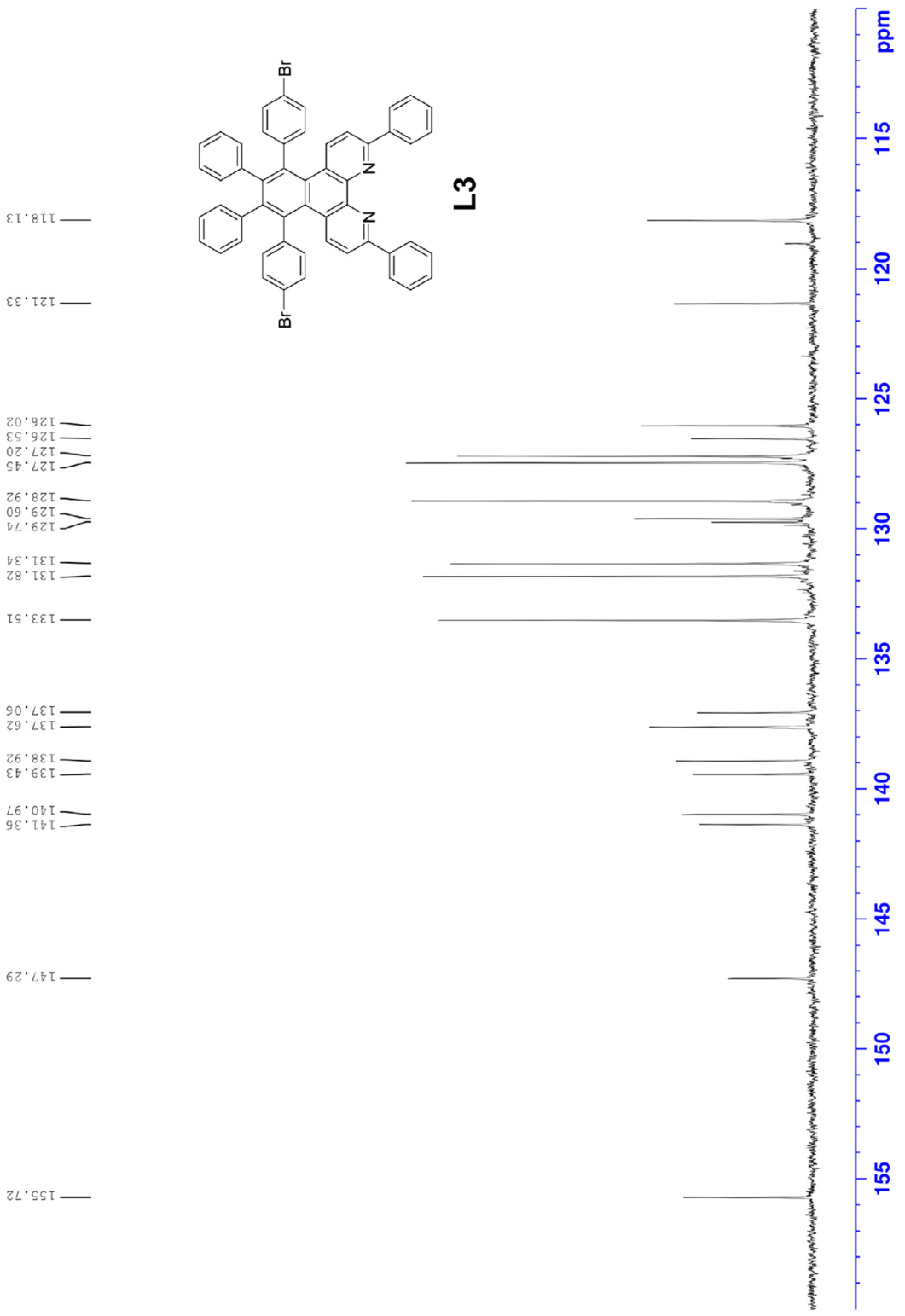

Figure S32. ^{13}C NMR spectrum of **L3** ($CDCl_3$).

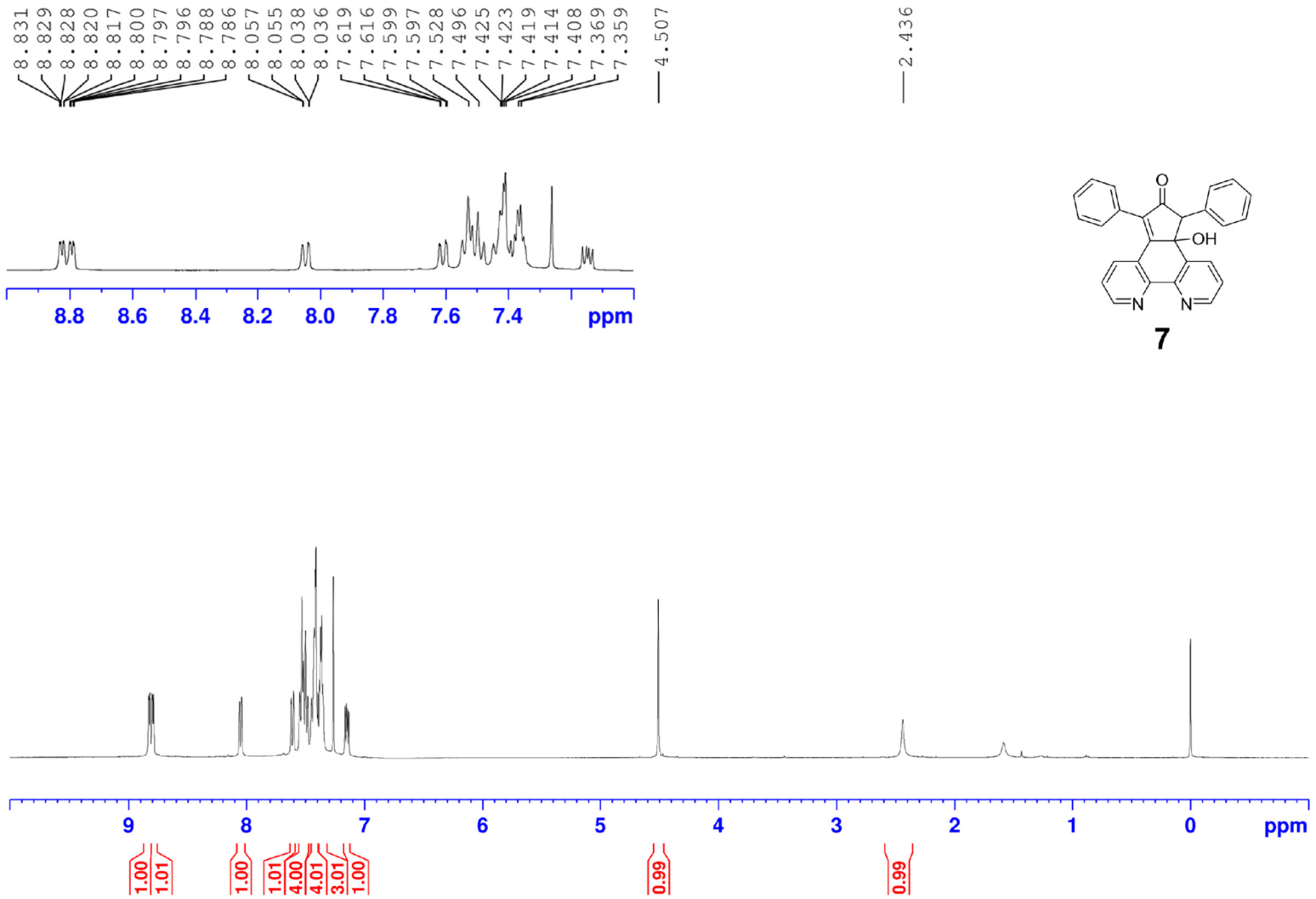

Figure S33. ^{1}H NMR spectrum of **7** ($CDCl_3$).

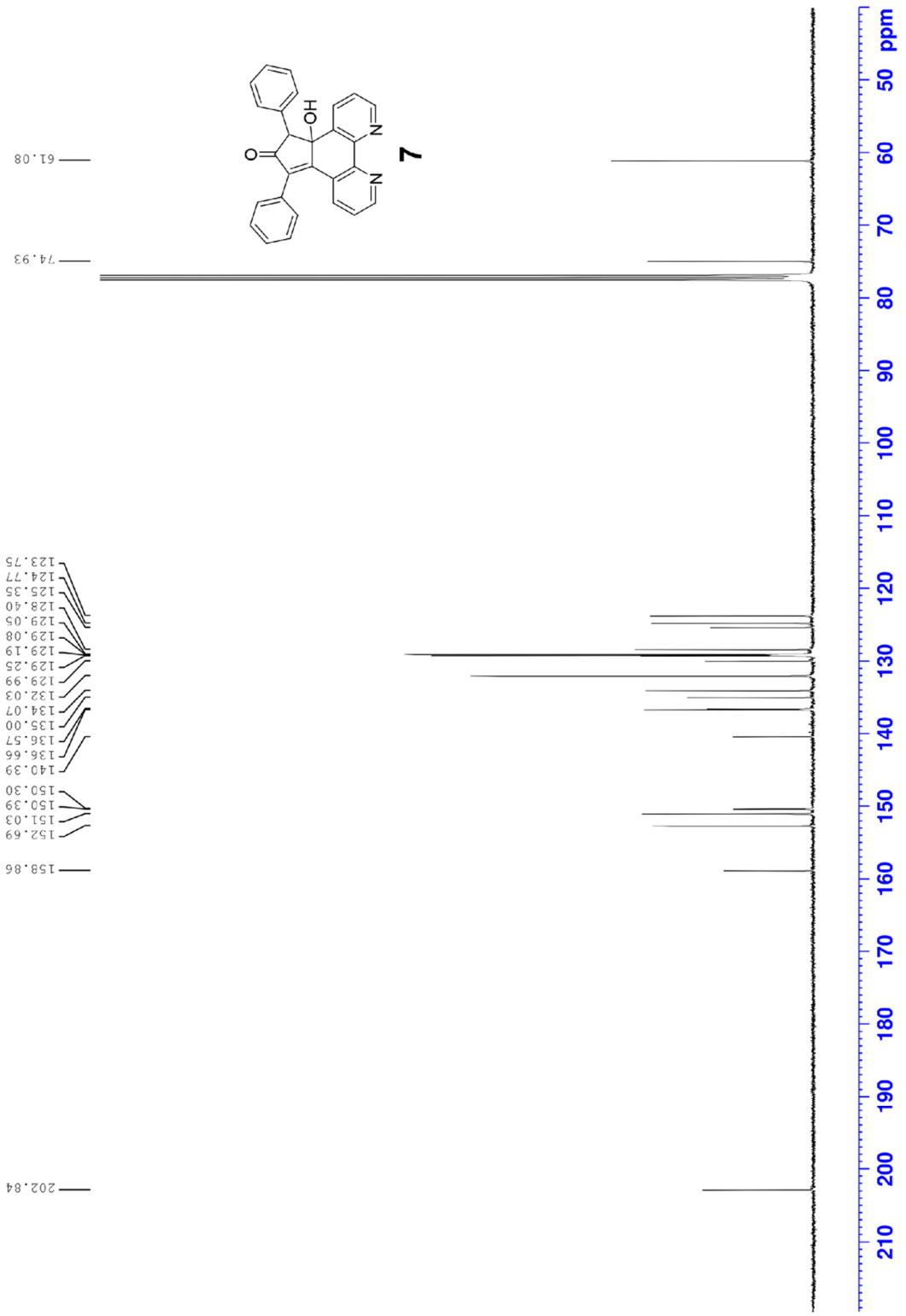

Figure S34. ^{13}C NMR spectrum of **7** ($CDCl_3$).

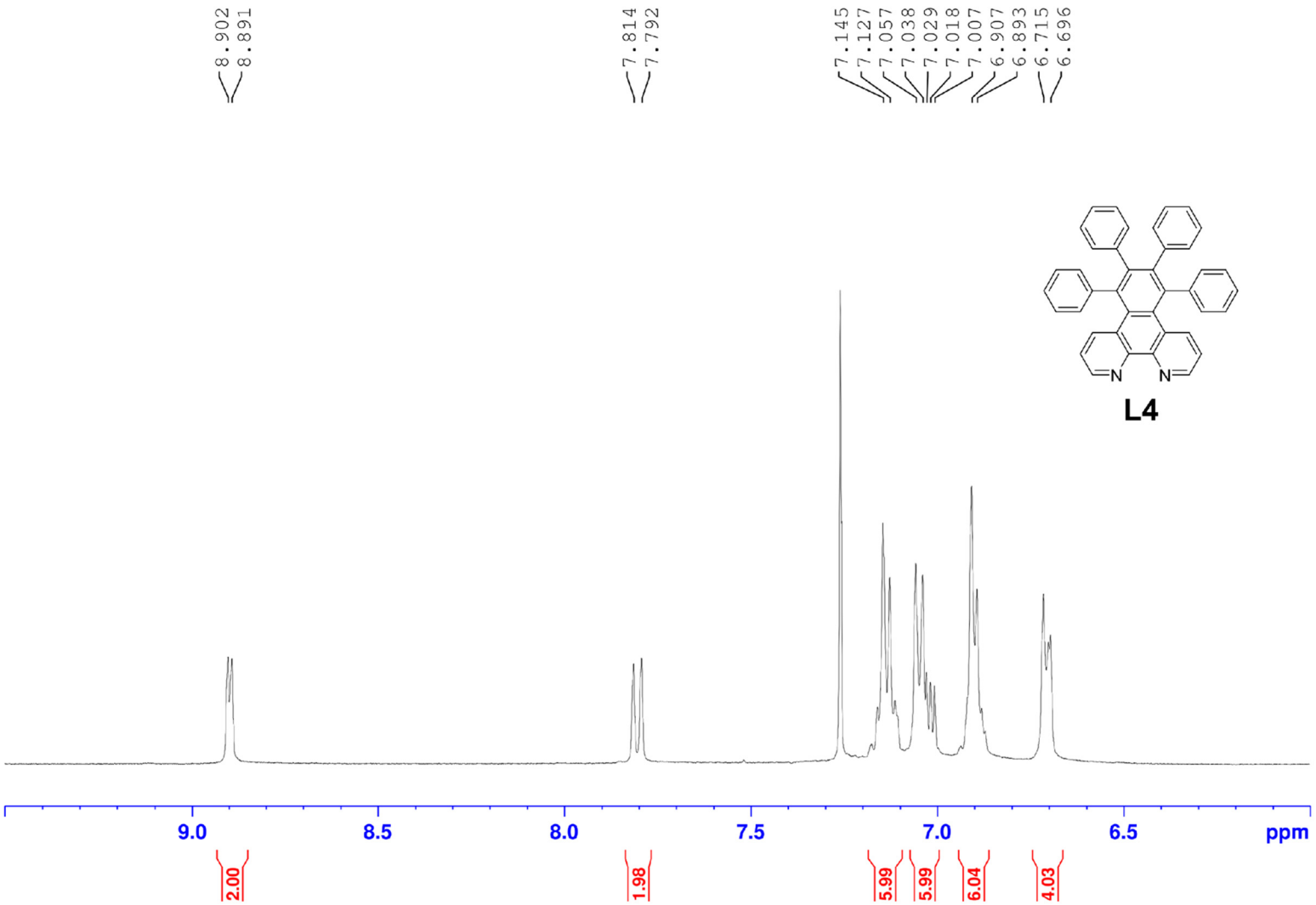

Figure S35. ^{1}H NMR spectrum of **L4** ($CDCl_3$).

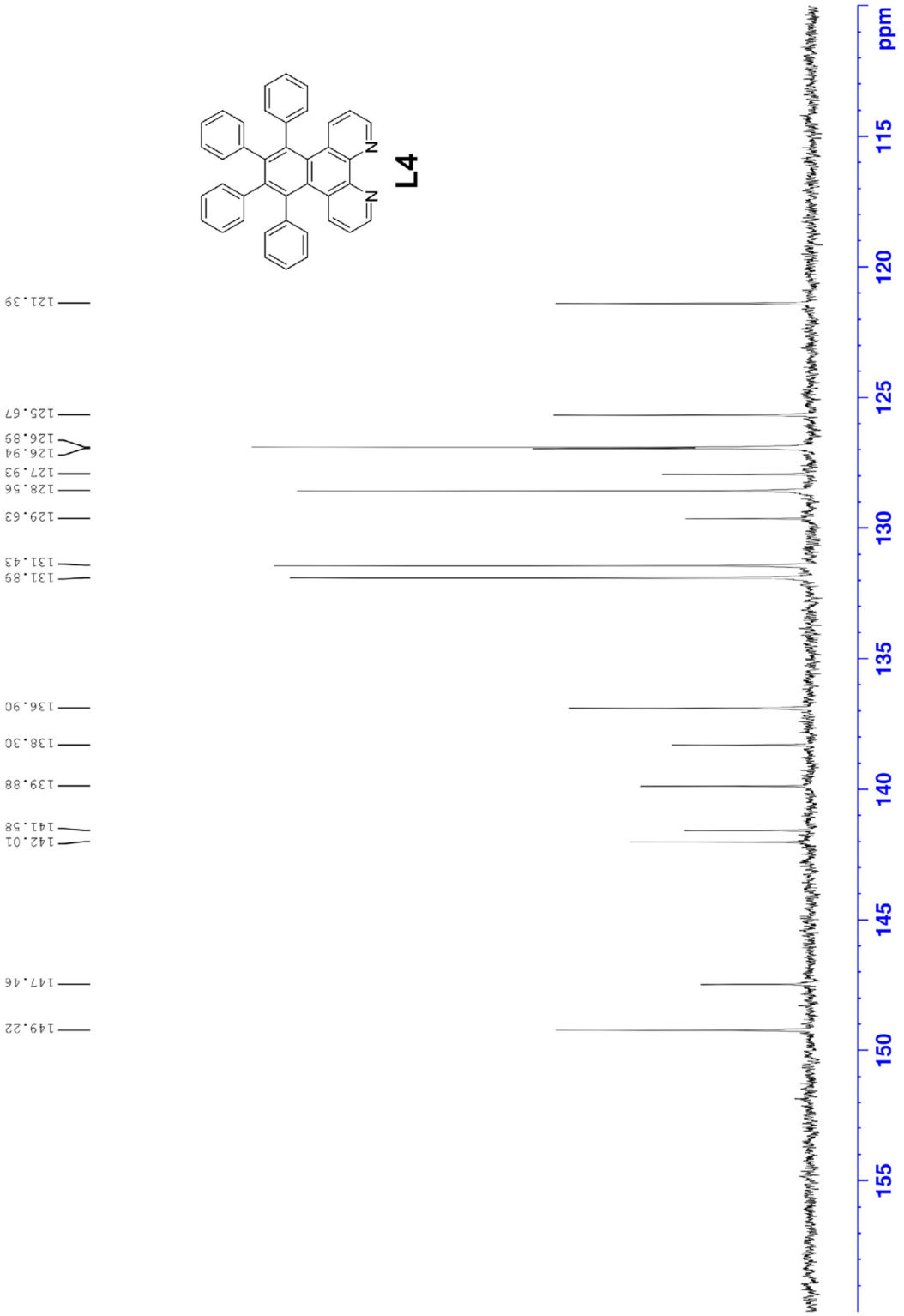

Figure S36. ^{13}C NMR spectrum of **L4** ($CDCl_3$).

3. References

[1] Y. Qin, L. Zhang, J. Lv, S. Luo, J.-P. Cheng, *Org. Lett.* **2015**, *17*, 1469−1472.

[2] J. Cai, C. A. Pignedoli, L. Talirz, P. Ruffieux, H. Söde, L. Liang, V. Meunier, R. Berger, R. Li, X. Feng, K. Müllen, R. Fasel, *Nat. Nanotechnol.* **2014**, *9*, 896−900. (b) T. H. Vo, M. Shekhirev, D. A. Kunkel, M. D. Morton, E. Berglund, L. Kong, P. M. Wilson, P. A. Dowben, A. Enders, A. Sinitskii, *Nat. Commun.* **2014**, *5*, 3189.

[3] K. Keiichi, S. Takahiro, T. Norihiro, S. Naoki, *Chem. Lett.* **2007**, *36*, 11222−1123.

[4] S. Jakobse, M. Tilset, *Tetrahedron Lett.* **2011**, *52*, 3072−3074.

[5] J. Frey, T. Kraus, V. Heitz, J.-P. Sauvage, *Chem. Eur. J.* **2007**, *13*, 7584−7594.

[6] Rigaku Oxford Diffraction (2015), Software CrysAlisPro 1.171.39.20a. Rigaku Corporation, Tokyo, Japan.

[7] G. M. Sheldrick, *Acta Crystallogr. Sect. A* **2015**, 71, 3−8.

[8] (a) Rigaku (2018). CrystalStructure. Version 4.3. Rigaku Corporation, Tokyo, Japan. (b) O. V. Dolomanov, L. J. Bourhis, R. J. Gildea, J. A. K. Howard and H. Puschmann, H. *J. Appl. Cryst.* **2009**, *42*, 339–341. (c) L. J. Bourhis, O. V. Dolomanov, R. J. Gildea, J. A. K. Howard and H. Puschmann, *Acta Crystallogr. Sect. A* **2015**, *71*, 59−75.

[9] G. M. Sheldrick, *Acta Crystallogr. C* **2015**, *71*, 3−8.

[10] (a) P. V. D. Sluis, A. L. Spek, *Acta Crystallogr. Sect. A* **1990**, *46*, 194. (b) A. L. Spek, *Acta Crystallogr. Sect. D* **2009**, *65*, 148−155.

[11] (a) M. Kato, K. Kimijima, M. Shibata, H. Notsu, K. Ogino, K. Inokuma, N. Ohta, H. Uehara, Y. Uemura, N. Oyaizu, T. Ohba, S. Takakusagi, K. Asakura, I. Yagi, *Phys. Chem. Chem. Phys.* **2015**, *17*, 8638−8641. (b) M. Kato, M. Muto, N. Matsubara, Y. Uemura, Y. Wakisaka, T. Yoneuchi, D. Matsumura, T. Ishihara, T. Tokushima, S. Noro, S. Takakusagi, K. Asakura, I. Yagi, *ACS Appl. Energy Mater.* **2018**, *1*, 2358−2364.

[12] (a) S. I. Zabinsky, J. J. Rehr, A. Ankudinov, R. C. Albers, M. J. Eller, *Phys. Rev. B* **1995**, *52*, 2995−3009. (b) J. J. Rehr, R. C. Albers, *Rev. Mod. Phys.* **2000**, *72*, 621−654.

[13] M. Moriya, R. Takahama, K. Kamoi, J. Ohyama, S. Kawashima, R. Kojima, M. Okada, T. Hayakawa, Y. Nabae, *J. Phys. Chem. C* **2020**, *124*, 20730−20735.

[14] (a) T. Taguchi, *AIP Conf. Proc.* **2006**, *882*, 162−164. (b) T. Taguchi, T. Ozawa, H. Yashiro, *Phys. Scr.* **2005**, *2005*, 205.